

Dynamic spectral co-clustering of directed networks to unveil latent community paths in VAR-type models

Younghoon Kim¹ and Changryong Baek^{*2}

¹Cornell University

²Sungkyunkwan University

February 18, 2025

Abstract

Identifying network Granger causality in large vector autoregressive (VAR) models enhances explanatory power by capturing complex interdependencies among variables. Instead of constructing network structures solely through sparse estimation of coefficients, we explore latent community structures to uncover the underlying network dynamics. We propose a dynamic network framework that embeds directed connectivity within the transition matrices of VAR-type models, enabling tracking of evolving community structures over time. To incorporate network directionality, we employ degree-corrected stochastic co-block models for each season or cycle, integrating spectral co-clustering with singular vector smoothing to refine latent community transitions. For greater model parsimony, we adopt periodic VAR (PVAR) and vector heterogeneous autoregressive (VHAR) models as alternatives to high-lag VAR models. We provide theoretical justifications for the proposed methodology and demonstrate its effectiveness through applications to the cyclic evolution of US nonfarm payroll employment and the temporal progression of realized stock market volatilities. Indeed, spectral co-clustering of directed networks reveals dynamic latent community trajectories, offering deeper insights into the evolving structure of high-dimensional time series.

Keywords—Community detection, dynamic network, stochastic block model, spectral clustering, periodic autoregression, heterogeneous autoregression

1 Introduction

The early concept of Granger causality (e.g., Granger; 1969) aims to determine whether a variable can be better explained by considering other exogenous or endogenous variables in a bivariate system, in terms of predictability. In low-dimensional extensions where the number of variables exceeds two, Eichler (2007) introduced a path diagram with nodes and edges based on a vector autoregressive (VAR) model. The diagram represents variables as nodes, connected by directed or undirected edges if an association exists, including their mediating variables, in a single graph. The

*Corresponding author. Email: crbaek@skku.edu, Department of Statistics, Sungkyunkwan University, 25-2, Sungkyunkwan-ro, Jongno-gu, Seoul, 03063, Korea.

goal is to identify significantly related endogenous variable pairs in a stationary large VAR model, known as network Granger causality (e.g., Chapter 3 in Shojaie and Fox; 2022).

Similarly to the low-dimensional case, the identification of non-zero paths in the VAR model is linked to the determination of causal relationships between variables through the embedded network (e.g., Brownlees et al.; 2018; Barigozzi et al.; 2023) in a high-dimensional regime. Unlike pairwise partial correlation in the Gaussian graphical model, which reveals only contemporaneous and undirected network topology (e.g., see Chapter 7.3 in Kolaczyk; 2009), the paths capture diachronic, directed relationships. The primary approach for learning high-dimensional graphs from transition matrices is Lasso estimation (e.g., Basu and Michailidis; 2015; Kock and Callot; 2015), assuming model sparsity. However, relying solely on sparsity to uncover network structure may be overly simplistic. For example, in follower-followed relationships (e.g., Twitter), financial spillover effects between corporations, or external stimulus propagation in the brain connectome, strong pairwise interactions may exist but simple sparse models may fail to capture.

The network autoregressive (NAR) model (e.g., Zhu et al.; 2017, 2019; Yin et al.; 2023) was developed to incorporate so-called “group” and “community” as variable clusters in time series models. Although its parameters are more restrictive than those of the sparse VAR model, the NAR model captures network effects within the transition matrix. A recent study by Zhu and Pan (2020) addressed heterogeneity within group effects in the NAR model, drawing inspiration from the Gaussian mixture model. Zhu et al. (2023) further extended the model to capture heterogeneity between groups. Separately, Knight et al. (2019) and Krampe (2019) proposed network-embedded Vector Autoregressive Moving Average (VARMA) models. More recently, Mantziou et al. (2023) introduced a variant incorporating time-varying connectivity in transition matrices, while Martin et al. (2024) proposed penalizing edges not identified as connected during VAR model estimation.

The NAR model variants above assume a known adjacency structure among all network nodes. For unknown group structures, these studies rely on iterative algorithms such as the EM algorithm, updating k -means clustering results at each step Zhu and Pan (2020); Zhu et al. (2023); Martin et al. (2024), and estimating model parameters repetitively, similar to panel data methods (e.g., Ando and Bai; 2016, 2017). However, embedding network structure in VAR transition matrices requires either model-wise restrictions (e.g., the number of parameters approximates the number of groups) or identification restrictions (e.g., normalizing adjacency matrices). Additionally, clustering is influenced by the choice of estimation method and tuning parameters such as Lasso estimation.

Using the stochastic block model (SBM, Holland et al.; 1983) addresses these NAR model issues by separating clustering from estimation. Moreover, if the focus is on the identification of group structure rather than graph learning, efficient clustering algorithms, such as spectral

*Community is more oriented towards network literature, while group is often used in time series modeling. In what follows, we will use both terms interchangeably.

clustering by Rohe et al. (2011), can be leveraged via the low-rank representation of constructed graphs. Among SBMs, the degree-corrected stochastic block model by Karrer and Newman (2011) is widely used to account for heterogeneity in communities. Hereafter, “SBM” will specifically refer to degree-corrected SBM. A recent study by Guðmundsson and Brownlees (2021) employed regularized Laplacian matrices, representing undirected graph connectivity (see Chapter 2.1 in Kolaczyk; 2009), derived from high-dimensional VAR transition matrices. A similar modeling approach was used in Brownlees et al. (2022) for panel data analysis.

Despite its advantages, the above approach has notable limitations. First, as seen in Guðmundsson and Brownlees (2021), SBMs in time series modeling can only represent *undirected* networks because normalized Laplacian matrices must be symmetrized for clustering. Since network Granger causality was originally developed to capture directed connectivity, symmetrization makes identifying directed relationships between variables difficult. More importantly, the model assumes a single network representation, meaning that the network structure remains identical across all lag orders. For example, Chen et al. (2022) adapted the SBM to capture the effects of the network in the NAR model, which remains within the VAR(1) framework. Similarly, Guðmundsson and Brownlees (2021) examined Granger causality using partitioned random graphs in all lag orders in VAR models. However, because all transition matrices were summed to construct a single graph, distinguishing different community structures over long lags was not possible. In other words, the varying networks across different lag orders cannot be identified.

To address the two issues above, we propose a dynamic network construction for VAR-type models using a sequence of directed blockmodels, which captures the evolution of community structures over a longer range. Specifically,

- We propose a spectral clustering approach for graphs modeled by the generalized stochastic co-blockmodel (ScBM), extending the degree-corrected stochastic co-blockmodel (e.g., Rohe et al.; 2016; Wang, Liang and Ji; 2020). By considering directed networks, the clustering results can capture network Granger causality. Additionally, defining the adjacency matrix with real values allows the blockmodel to represent VAR transition matrices. As with SBM above, the term ScBM will refer to the *degree-corrected stochastic co-blockmodel* throughout this paper, while *generalized ScBM* will be specified only when necessary.
- We extend the ordinary VAR model to two high-dimensional VAR-type models. First, we use periodic vector autoregressive models (PVAR; Baek et al.; 2017, 2018) to model cyclic changes in community structures through their transition matrices. Second, we incorporate vector heterogeneous autoregressive models (VHAR; Cubadda et al.; 2017; Baek and Park; 2021), allowing transition matrices to reflect daily, weekly, and monthly community structures.

- We introduce a variant of eigenvector smoothing, a method for constructing dynamic networks with evolving community structures (e.g., Liu et al.; 2018; Lei et al.; 2020; Ji et al.; 2022). For directed random networks, this variant balances the left and right singular vectors of the ScBM, ensuring smooth transitions in community structures across seasons and cycles.

The rest of the paper is organized as follows. Section 2 introduces the time series model of interest and its corresponding population dynamic networks. Section 3 describes the spectral co-clustering algorithm for identifying community structures. Section 4 presents the consistency theory, while Section 5 details numerical experiments. Section 6 illustrates two data applications, and Section 7 concludes the study.

Notation: Throughout the paper, we define the ℓ_2 norm as $\|v\|_2 = \sqrt{\sum_{i=1}^d v_i^2}$. For a matrix M , we denote the spectral, Frobenius, matrix- ℓ_1 (maximum absolute column sum), and matrix- ∞ (maximum absolute row sum) norms as $\|M\|$, $\|M\|_F$, $\|M\|_1$, $\|M\|_\infty$, respectively. \mathbb{N}^+ implies a set of natural number including zero.

2 Model description

Let Y_t be a q -dimensional centered time series. The vector autoregressive model of lag order p , denoted as VAR(p), is defined as

$$Y_t = \sum_{h=1}^p \Phi_h Y_{t-h} + \varepsilon_t, \quad \varepsilon_t \sim \text{WN}(0, \Sigma_\varepsilon), \quad t = 1, \dots, T, \quad (1)$$

The number of variables pq^2 may exceed the sample size T , making VAR(p) a high-dimensional time series model (e.g., Basu and Michailidis; 2015; Kock and Callot; 2015). We use VAR(p) as a baseline to introduce other time series models.

The periodic vector autoregressive model with season s , denoted as PVAR(s), is defined as

$$Y_t = \sum_{h=1}^{p_m} \Phi_{h,m} Y_{t-h} + \varepsilon_{t,m}, \quad \varepsilon_{t,m} \sim \text{WN}(0, \Sigma_{\varepsilon,m}), \quad t = 1, \dots, T, \quad (2)$$

where p_m is the lag order during season $m = 1, \dots, s$. The lag order p_m may vary across seasons. Note that when $s = 1$, PVAR(s) reduces to VAR(p). Following the convention for linking seasons and sample lengths (e.g., Baek et al.; 2017; Boubacar Maïnassara and Ursu; 2023), the time index t in (2) can be rewritten as $t = m + ns$, where $n \in \mathbb{Z}$ represents the cycle. This allows us to express (2) as

$$Y_{m+ns} = \sum_{h=1}^{p_m} \Phi_{h,m} Y_{m+ns-h} + \varepsilon_{m+ns,m}, \quad \varepsilon_{m+ns,m} \sim \text{WN}(0, \Sigma_{\varepsilon,m}). \quad (3)$$

The both representations (2) and (3) will be used to indicate the same model throughout the paper.

A vector heterogeneous autoregressive (VHAR) model is defined as

$$Y_t = \Phi_{(d)} Y_{t-1}^{(d)} + \Phi_{(w)} Y_{t-1}^{(w)} + \Phi_{(m)} Y_{t-1}^{(m)} + \varepsilon_t, \quad \varepsilon_t \sim \text{WN}(0, \Sigma_\varepsilon), \quad t = 1, \dots, T, \quad (4)$$

where (d) , (w) , and (m) represent one day, one week (five trading days, excluding weekends), and one month (22 trading days, excluding weekends), respectively. These components are computed as averages of Y_t over their respective periods:

$$Y_t^{(d)} = Y_t, \quad Y_t^{(w)} = \frac{1}{5} \sum_{h=0}^4 Y_{t-h}, \quad Y_t^{(m)} = \frac{1}{22} \sum_{h=0}^{21} Y_{t-h}. \quad (5)$$

Here, the daily, weekly, and monthly dependencies serve as proxies for short-, medium-, and long-term effects, respectively (e.g., Clements and Preve; 2021), capturing long-memory behavior in the series. Additionally, the VHAR model (4) can be expressed as a VAR(22) model with the following coefficient restrictions:

$$\Phi_1 = \Phi_{(d)} + \frac{1}{5} \Phi_{(w)} + \frac{1}{22} \Phi_{(m)}, \quad \Phi_2 = \dots = \Phi_5 = \frac{1}{5} \Phi_{(w)} + \frac{1}{22} \Phi_{(m)}, \quad \Phi_6 = \dots = \Phi_{22} = \frac{1}{22} \Phi_{(m)}. \quad (6)$$

This restriction reduces the number of parameters from $22q^2 + \binom{q}{2}$ to $3q^2 + \binom{q}{2}$, making the model parsimonious while effectively capturing long-term dependencies. Due to this advantage, the empirical effectiveness of the VHAR model in forecasting has been widely demonstrated (e.g., Wang, Lu, He and Ma; 2020; Zhang et al.; 2020; Wilms et al.; 2021). Furthermore, throughout this study, we will show that the daily, weekly, and monthly terms in VHAR behave similarly to the three seasonal components in PVAR-based models. Thus, in the context of VHAR-based models, the term *seasons* refers to these three time scales.

To explain the graph structure embedded in the VAR, PVAR, and VHAR models, we follow Brownlees et al. (2022); Guðmundsson and Brownlees (2021) and Rohe et al. (2016) for model construction. This approach is similar to the standard SBM framework (e.g., Karrer and Newman; 2011), but it extends to directed graphs by distinguishing between sending and receiving node communities while also accounting for connectivity strength beyond binary connections.

From a modeling perspective, the random graph at season m , denoted as $\mathcal{G}_m = (\mathcal{V}_m, \mathcal{E}_m, \mathcal{W}_m)$, consists of three components. The set of nodes is $\mathcal{V}_m = \{1, \dots, q\}$, partitioned into K_{m_y} sending communities $\mathcal{V}_{m,1}, \dots, \mathcal{V}_{m,K_{m_y}}$ and K_{m_z} receiving communities $\mathcal{V}_{m,1}, \dots, \mathcal{V}_{m,K_{m_z}}$. The numbers of sending and receiving communities, K_{m_y} and K_{m_z} , are not necessarily equal. The set of edges, $\mathcal{E}_m \subset \mathcal{V}_m \times \mathcal{V}_m$, represents directed node pairs (i, j) , where the connectivity strength is denoted by $[w_m]_{ij}$. The weight set is given by

$$\mathcal{W}_m = \{[w_m]_{ij} \in \mathbb{R} \setminus \{0\} : (i, j) \in \mathcal{E}_m\}.$$

The adjacency matrix $A_m \in \mathbb{R}^{q \times q}$ at season m has entries satisfying $[w_m]_{ij} \neq 0$ if $(i, j) \in \mathcal{E}_m$ and zero otherwise. The weights $[w_m]_{ij}$ are assumed to be independently drawn from a distribution

supported on the interval $[w_{m,l}, w_{m,u}]$, where $0 < w_{m,l} < w_{m,u}$, with mean μ_m and variance σ_m^2 . Define $B_m \in [0, 1]^{K_{y_m} \times K_{z_m}}$ as the community link matrix, representing the expected number of links between communities. Following the SBM assumption, the probability of a directed edge from node i to node j is given by

$$\mathbb{P}((i, j) \in \mathcal{E}_m) = \mathbb{P}([A_m]_{ij} \neq 0) = [\Theta_m^y]_{ii} [\Theta_m^z]_{jj} [B_m]_{y_i z_j},$$

for $y_i = 1, \dots, K_{m_y}$ and $z_j = 1, \dots, K_{m_z}$, where $[\Theta_m^y]_{ii}$ and $[\Theta_m^z]_{jj}$ are diagonal entries of the matrices Θ_m^y and Θ_m^z , representing the propensity of nodes i and j at season m . For identifiability, we impose the constraints

$$\sum_{i \in \mathcal{V}_{m,k}} [\Theta_m^y]_{ii} = 1, \quad k = 1, \dots, K_{m_y}, \quad \text{and} \quad \sum_{j \in \mathcal{V}_{m,k}} [\Theta_m^z]_{jj} = 1, \quad k = 1, \dots, K_{m_z}.$$

The population adjacency matrix \mathcal{A}_m is given by

$$\mathcal{A}_m := \mathbb{E}[A_m] = \mu_m \Theta_m^y Y_m B_m Z_m' \Theta_m^z, \quad (7)$$

where $Y_m \in \{0, 1\}^{q \times K_{y_m}}$ and $Z_m \in \{0, 1\}^{q \times K_{z_m}}$ are the sending and receiving membership matrices, respectively.

Finally, we introduce the transition matrices of the time series models. First, consider the VAR(p) model and assume that for each lag order $h = 1, \dots, p$, the embedded network structure follows the ScBM. That is,

$$\Phi_h = \phi_h (P_h^\tau)^{-1/2} A_h' (O_h^\tau)^{-1/2}, \quad h = 1, \dots, p, \quad (8)$$

where $P_h^{\tau_h}$ and $O_h^{\tau_h}$ are diagonal matrices with

$$[P_h^\tau]_{jj} = \sum_k [A_h']_{kj} + \tau_h, \quad [O_h^\tau]_{ii} = \sum_k [A_h']_{ik} + \tau_h,$$

where τ_h is the average out-degree

$$\tau_h := \frac{1}{q} \sum_k [A_h']_{ik},$$

used for regularization (e.g., Chaudhuri et al.; 2012; Qin and Rohe; 2013). Adding the average connectivity strength to the node degree improves clustering results, particularly when node degrees are heterogeneous. The numbers of sending and receiving communities, K_{y_m} and K_{z_m} , may differ, but only the smaller number appears as a result of singular value decomposition (SVD). The scalar $\phi_h \in \mathbb{R}$ scales the VAR(p) coefficients in (8) to ensure model stability, that is, satisfying

$$\det(I - \Phi_1 z - \dots - \Phi_p z^p) \neq 0 \quad \text{for } |z| \leq 1.$$

Note that the adjacency matrix A_h is transposed, and the in- and out-degree matrices are swapped compared to the conventional representation. This adjustment ensures that (8) correctly forms

the VAR transition matrix, aligning with the temporal order and physical interpretation—where variables in the previous time point (columns) are associated with variables in the next time point (rows). If the in-degrees and out-degrees are identical for all Φ_h , the model with transition matrices (8) reduces to SB-VAR as proposed by Guðmundsson and Brownlees (2021). Hereafter, we refer to the model as ScBM-VAR when the VAR model assumes transition matrices at each lag follow the ScBM structure as in (8).

By applying the ScBM-VAR framework to the PVAR model with seasonality s , we obtain the ScBM-PVAR model. The transition matrices are given by

$$\Phi_{h,m} = \phi_{h,m} (P_{h,m}^{\tau_{h,m}})^{-1/2} A'_{h,m} (O_{h,m}^{\tau_{h,m}})^{-1/2}, \quad h = 1, \dots, p_m, \quad (9)$$

where $P_{h,m}^{\tau_{h,m}}$, $O_{h,m}^{\tau_{h,m}}$, $\tau_{h,m}$, and $\phi_{h,m}$ are defined similarly to (8) across seasons $m = 1, \dots, s$. Similarly, the ScBM-VHAR model is defined by transition matrices of the form

$$\Phi_{(h)} = \phi_{(h)} (P_{(h)}^{\tau_{(h)}})^{-1/2} A'_{(h)} (O_{(h)}^{\tau_{(h)}})^{-1/2}, \quad h = d, w, m. \quad (10)$$

The matrices and constants $P_{(h)}^{\tau_{(h)}}$, $O_{(h)}^{\tau_{(h)}}$, $\tau_{(h)}$, and $\phi_{(h)}$ are defined as in (8) across the three seasons: daily ($h = d$), weekly ($h = w$), and monthly ($h = m$).

Remark 2.1 Note that for blockmodels, the in- and out-degrees, obtained by summing degrees within the same community and normalizing by the same quantities, are identical because the adjacency matrix values are either zero or one. This property may be restrictive for VAR transition matrices, where entries can take any real values. This limitation can be addressed by using Poisson-edge graphs instead of Bernoulli-edge graphs during the sampling step. Specifically, allowing random samples to overlap at the same entries and summing the counts at each component enables adjacency matrix entries to take values greater than zero or one. Theorem 7 in Rohe et al. (2018) establishes a coupling between Poisson-edge and Bernoulli-edge graph sampling. Indeed, random graph packages such as `fastRG` by Rohe et al. (2018) predominantly adopt Poisson-edge sampling to address this issue. However, we follow the framework of Guðmundsson and Brownlees (2021) by imposing uniformly random edge weights.

3 Spectral co-clustering algorithms

In this section, we describe the algorithm used for the ScBM-VAR-type models introduced in Section 2. We first outline the algorithm for detecting communities based on regularized Laplacian matrices derived from the underlying VAR models. The algorithm is then extended to incorporate seasonal models by clustering on the regularized Laplacian matrices separately and smoothing their singular vectors to ensure they remain as close to each other as possible.

3.1 Spectral co-clustering for ScBM-VAR

The spectral co-clustering method proposed by Rohe et al. (2016) performs directional clustering on the regularized asymmetric graph Laplacian matrix. The *VAR Blockbuster algorithm* in Guðmundsson and Brownlees (2021), based on spectral clustering by Rohe et al. (2011), normalizes row-wise eigenvectors from the estimated symmetrized Laplacian matrices obtained by summing VAR transition matrices and their transposes. In contrast, the spectral co-clustering algorithm applies row-wise normalization separately to the left and right singular vectors. These singular vectors are derived from the sum of transition matrices within the same seasons. For simplicity, we explain the spectral co-clustering algorithm for the ScBM-VAR model.

1. Estimate transition matrices $\hat{\Phi}_h$, $h = 1, \dots, p$, of ScBM-VAR(p) model via ordinary least squares (OLS) method.
2. From the autoregressive matrix $\hat{\Phi} = \sum_{h=1}^p \hat{\Phi}'_h$, construct the regularized Laplacian matrix $\hat{L} = (\hat{O}^\tau)^{-1/2} \hat{\Phi} (\hat{P}^\tau)^{-1/2}$, where \hat{O}^τ and \hat{P}^τ are diagonal matrices with $[\hat{O}^\tau]_{ii} = \sum_k [\hat{\Phi}]_{ik} + \tau$ and $[\hat{P}^\tau]_{jj} = \sum_k [\hat{\Phi}]_{kj} + \tau$, where $\tau = q^{-1} \sum_k [\hat{\Phi}]_{ik}$.
3. Compute the top K left and right singular vectors, denoted as $\hat{X}_L \in \mathbb{R}^{q \times K}$ and $\hat{X}_R \in \mathbb{R}^{q \times K}$ respectively, where $K = \min(K_y, K_z)$.
4. Normalize each row of \hat{X}_L and \hat{X}_R to have a unit length. That is, define $\hat{X}_L^* \in \mathbb{R}^{q \times K}$ and $\hat{X}_R^* \in \mathbb{R}^{q \times K}$ such that

$$[\hat{X}_L^*]_i = \frac{[\hat{X}_L]_i}{\|[\hat{X}_L]_i\|_2}, \quad [\hat{X}_R^*]_i = \frac{[\hat{X}_R]_i}{\|[\hat{X}_R]_i\|_2}, \quad i = 1, \dots, q. \quad (11)$$

5. If $K_y = K_z = K$, then run k -means clustering on rows of

$$(\hat{X}_L^* \quad \hat{X}_R^*) \in \mathbb{R}^{q \times 2K}.$$

Otherwise, run k -means clustering separately on rows of \hat{X}_L^* and \hat{X}_R^* using K_y and K_z clusters.

3.2 Spectral co-clustering for ScBM-PVAR

We extend the spectral co-clustering algorithm for the ScBM-VAR model by incorporating singular vector smoothing, inspired by the eigenvector smoothing approach introduced in *PisCES* (Liu et al.; 2018). It ensures smooth transitions in community structures across seasons. We assume that for $m = 2, \dots, s$, the community structure of receiving nodes in season $m - 1$ is identical to that of sending nodes in season m . Similarly, the structures of the receiving and sending node communities in the last season ($m = s$) and the first season ($m = 1$) are also assumed to be identical. This constraint is not required for the modeling step in Section 2 but ensures a smooth cyclic evolution of

the model across seasons. Consequently, in addition to $K_m = \min(K_{m_y}, K_{m_z})$ imposed in spectral co-clustering for ScBM-VAR in Section 3.1, we assume that $K_{(m-1)_z} = K_{m_y}$ for $m = 2, \dots, s$, and $K_{s_z} = K_{1_y}$. For simplicity, we set $p_m = p$ for all $m = 1, \dots, s$. However, this approach can be generalized to other ScBM-PVAR models with arbitrary lag orders for each season. The steps of the algorithm are as follows.

1. Estimate transition matrices $\hat{\Phi}_{m,h}$, $h = 1, \dots, p$, $m = 1, \dots, s$ of ScBM-PVAR(s) model via OLS method.
2. From the seasonal autoregressive matrices $\hat{\Phi}_m = \sum_{h=1}^p \hat{\Phi}'_{m,h}$, construct the regularized Laplacian matrices $\hat{L}_m = (\hat{O}_m^{\tau_m})^{-1/2} \hat{\Phi}_m (\hat{P}_m^{\tau_m})^{-1/2}$, where $\hat{O}_m^{\tau_m}$ and $\hat{P}_m^{\tau_m}$ are diagonal matrices with $[\hat{O}_m^{\tau_m}]_{ii} = \sum_k [\hat{\Phi}_m]_{ik} + \tau_m$ and $[\hat{P}_m^{\tau_m}]_{jj} = \sum_k [\hat{\Phi}_m]_{kj} + \tau_m$, where $\tau_m = q^{-1} \sum_i [\hat{\Phi}_m]_{ik}$.
3. Compute the top K_{y_m} left and K_{z_m} right singular vectors $\hat{X}_L \in \mathbb{R}^{q \times K_{y_m}}$ and $\hat{X}_R \in \mathbb{R}^{q \times K_{z_m}}$, where $K_{z_{m-1}} = K_{y_m}$, $m = 2, \dots, s$, and $K_{z_s} = K_{y_1}$ are assumed.
4. Run PisCES algorithm by Liu et al. (2018) for two sequences of singular vectors separately;
 - a. For each season m , set $U_{m,L} = \hat{X}_{m,L} \hat{X}'_{m,L}$, where $\hat{X}_{m,L}$ and $\hat{X}_{m,R}$ are K_{y_m} left and K_{z_m} right SVD column vectors of \hat{L}_m , $m = 1, \dots, s$.
 - b. Set $\bar{U}_{m,L}^0 = U_{m,L}$ and $\bar{U}_{m,R}^0 = U_{m,R}$, $m = 1, \dots, s$.
 - c. For $l = 0, 1, \dots$, repeat (12)–(14) for the left SVD column vectors till convergence,

$$\bar{U}_{1,L}^{(l+1)} = \Pi(U_{1,L} + \alpha \bar{U}_{2,L}^{(l)}; K_{y_1}), \quad (12)$$

$$\bar{U}_{m,L}^{(l+1)} = \Pi(\alpha \bar{U}_{m-1,L}^{(l)} + U_{m,L} + \alpha \bar{U}_{m+1,L}^{(l)}; K_{y_m}), \quad m = 2, \dots, s-1, \quad (13)$$

$$\bar{U}_{s,L}^{(l+1)} = \Pi(\alpha \bar{U}_{s-1,L}^{(l)} + U_{s,L}; K_{y_s}), \quad (14)$$

where $\alpha > 0$ is the tuning parameter, which is more discussed in Section 3.4 and

$$\Pi(M; K) = \sum_{k=1}^K \nu_k \nu'_k,$$

where ν_1, \dots, ν_K are the K leading eigenvectors of matrix M .

- d. For $l = 0, 1, \dots$, repeat (15)–(17) for the right SVD column vectors till convergence,

$$\bar{U}_{1,R}^{(l+1)} = \Pi(U_{1,R} + \alpha \bar{U}_{2,R}^{(l)}; K_{z_1}), \quad (15)$$

$$\bar{U}_{m,R}^{(l+1)} = \Pi(\alpha \bar{U}_{m-1,R}^{(l)} + U_{m,R} + \alpha \bar{U}_{m+1,R}^{(l)}; K_{z_m}), \quad m = 2, \dots, s-1, \quad (16)$$

$$\bar{U}_{s,R}^{(l+1)} = \Pi(\alpha \bar{U}_{s-1,R}^{(l)} + U_{s,R}; K_{z_s}). \quad (17)$$

The method for finding series of numbers of communities $(K_{y_1}, \dots, K_{y_s})$ and $(K_{z_1}, \dots, K_{z_s})$ is discussed in Remark 3.2.

5. Define $\bar{U}_{m,L} = \bar{X}_{m,L}\bar{X}'_{m,L}$ and $\bar{U}_{m,R} = \bar{X}_{m,R}\bar{X}'_{m,R}$. Normalize each row of $\bar{X}_{m,L}$ and $\bar{X}_{m,R}$ to have a unit length similar to (11). Denote the normalized column vectors by $\hat{X}_{m,L}^*$ and $\hat{X}_{m,R}^*$, $m = 1, \dots, s$.
6. From $(\hat{X}_{1,L}^*, \hat{X}_{1,R}^*)$ to $(\hat{X}_{s,L}^*, \hat{X}_{s,R}^*)$, apply k -means clustering on the staggered paired rows, pairwise. Specifically, for $K_{z_{m-1}} = K_{y_m} = K$ with $m = 2, \dots, s$, and $K_{z_s} = K_{y_1} = K$, perform k -means clustering on the rows of

$$(\hat{X}_{m-1,R}^* \quad \hat{X}_{m,L}^*) \in \mathbb{R}^{q \times 2K}, \quad m = 2, \dots, s, \quad (\hat{X}_{s,R}^* \quad \hat{X}_{1,L}^*) \in \mathbb{R}^{q \times 2K}.$$

Remark 3.1 Unlike eigenvalue decomposition, where columns of orthogonal vectors can always be found, SVD produces left and right singular vectors that are nearly, but not exactly, orthogonal. Nevertheless, many related studies including those on sparse SVD (e.g., Shen and Huang; 2008; Witten et al.; 2009), allow for such approximations with algorithms designed to converge in most practical cases.

3.3 Spectral co-clustering for ScBM-VHAR

The spectral co-clustering and PisCES methods for ScBM-VHAR follow the same approach as for ScBM-PVAR, treating it as a special case with three seasons: $m = 1, 2, 3$, corresponding to daily (d), weekly (w), and monthly (m), respectively. However, there is a key difference. In ScBM-PVAR, the networks across seasons are assumed to be cyclic, meaning the group structure of the right singular vectors in the last season is identical to that of the left singular vectors in the first season. In contrast, ScBM-VHAR assumes a transient community structure, where these structures are not necessarily identical. That is, $K_{z(m)} = K_{y(d)}$ is not required. The algorithm for ScBM-VHAR (4) with (10) follows the approach in Section 3.2, with Steps 1, 2, and 6 replaced by:

1. Estimate transition matrices $\hat{\Phi}_{(d)}, \hat{\Phi}_{(w)}, \hat{\Phi}_{(m)}$ of ScBM-VHAR model (4) via OLS method.
2. Construct seasonal autoregressive matrices $\hat{\Phi}_1 = \hat{\Phi}'_{(d)}, \hat{\Phi}_2 = \hat{\Phi}'_{(w)}$, and $\hat{\Phi}_3 = \hat{\Phi}'_{(m)}$ and regard them as seasonal autoregressive matrices for three seasons.
6. From $(\hat{X}_{(d),L}^*, \hat{X}_{(d),R}^*)$ to $(\hat{X}_{(m),L}^*, \hat{X}_{(m),R}^*)$, apply k -means clustering on the staggered rows with pairs of $(\{(d), R\}, \{(w), L\})$ and $(\{(w), R\}, \{(m), L\})$, and $\{(d), L\}$ and $\{(m), R\}$, separately,

$$\hat{X}_{(d),L}^* \in \mathbb{R}^{q \times K}, \quad (\hat{X}_{(d),R}^* \quad \hat{X}_{(w),L}^*) \in \mathbb{R}^{q \times 2K}, \quad (\hat{X}_{(w),R}^* \quad \hat{X}_{(m),L}^*) \in \mathbb{R}^{q \times 2K}, \quad \hat{X}_{(m),R}^* \in \mathbb{R}^{q \times K},$$

where $K_{y(d)} = K$, $K_{z(d)} = K_{y(w)} = K$, $K_{y(w)} = K_{z(w)} = K$, and $K_{z(m)} = K$, respectively.

3.4 Cross-validation for PisCES smoothing parameter

The smoothing parameter in PisCES, when applied to ScBM-PVAR and ScBM-VHAR, plays a central role in finite-sample performance. Here, we introduce a cross-validation scheme for selecting the optimal tuning parameter.

1. Randomly divide $\binom{q}{2} - q$ dyads into M folds for indexing the arrays of the autoregressive matrices $\hat{\Phi}_m$, excluding diagonal indices.
2. For each fold $\ell = 1, \dots, M$, from $\hat{\Phi}_m \in \mathbb{R}^{q \times q}$, let

$$[\hat{\Phi}_m^{(\ell)}]_{ij} = \begin{cases} [\hat{\Phi}_m]_{ij}, & \text{if } (i, j, m) \in \ell, \\ 0, & \text{otherwise,} \end{cases}$$

and $\tilde{\Phi}_m^{(\ell)}$ be the result of matrix completion, e.g. Section 2.3 in Li et al. (2020), by applying SVD

$$\tilde{\Phi}_m^{(\ell)} := \frac{1}{0.9} \hat{W}_m^{(\ell)} \hat{D}_m^{(\ell)} \hat{V}_m^{(\ell)'}, \quad m = 1, \dots, s, \quad (18)$$

where $\hat{W}_m^{(\ell)}$ and $\hat{V}_m^{(\ell)}$ are K left and right SVD columns of $\hat{\Phi}_m^{(\ell)}$ with $K = \min(K_{y_m}, K_{z_m})$, and $D_m^{(\ell)}$ is diagonal with K singular values of $\hat{\Phi}_m^{(\ell)}$.

3. Let $\bar{U}_{m,L}^{(\alpha,\ell)}$ and $\bar{U}_{m,R}^{(\alpha,\ell)}$ be the result of PisCES algorithm with the completed Laplacian matrices $\tilde{\Phi}_m^{(\ell)}$ for a fixed α . Then compute node-community incidence vectors $y_m^{(\alpha,\ell)} = (y_{m,1}^{(\alpha,\ell)}, \dots, y_{m,q}^{(\alpha,\ell)})'$ and $z_m^{(\alpha,\ell)} = (z_{m,1}^{(\alpha,\ell)}, \dots, z_{m,q}^{(\alpha,\ell)})'$, $m = 1, \dots, s$.
4. Compute $\hat{\theta}_{m,i}^{(y,\alpha,\ell)} := \sum_k [\tilde{\Phi}_m^{(\alpha,\ell)}]_{ik}$, $\hat{\theta}_{m,j}^{(z,\alpha,\ell)} := \sum_k [\tilde{\Phi}_m^{(\alpha,\ell)}]_{kj}$, and

$$[\hat{B}_m^{(\alpha,\ell)}]_{kr} = \frac{\sum_{(i,j): y_{m,i}^{(\alpha,\ell)}=k, z_{m,i}^{(\alpha,\ell)}=r} [\tilde{\Phi}_m^{(\ell)}]_{ij}}{\sum_{(i,j): y_{m,i}^{(\alpha,\ell)}=k, z_{m,i}^{(\alpha,\ell)}=r} (\hat{\theta}_{m,i}^{(y,\alpha,\ell)} \cdot \hat{\theta}_{m,j}^{(z,\alpha,\ell)})},$$

$$[\hat{P}_m^{(\alpha,\ell)}]_{ij} = \hat{\theta}_{m,i}^{(y,\alpha,\ell)} \cdot \hat{\theta}_{m,j}^{(z,\alpha,\ell)} \cdot [\hat{B}_m^{(\alpha,\ell)}]_{y_{m,i}^{(\alpha,\ell)} z_{m,j}^{(\alpha,\ell)}}.$$

5. Compute a quadratic approximation of von Neumann entropy for the directed networks (e.g., equation (10) in Ye et al.; 2014) using

$$H(\ell, \alpha) = \sum_{m=1}^s \frac{\text{Tr}(\hat{\Phi}_m)}{q} \left(1 - \frac{\text{Tr}(\hat{P}_m^{(\alpha,\ell)})}{q} \right),$$

where $\text{Tr}(M)$ denotes the trace of matrix M . Select the value of α that minimizes $\sum_{\ell=1}^M H(\ell, \alpha)$ over all candidate values.

Remark 3.2 The number of communities in ScBM-VAR-type models can be estimated using scree plots by identifying points where the slope of eigenvalue differences changes significantly. However,

we can only determine the minimum numbers of communities by $K_m = \min\{K_{y_m}, K_{z_m}\}$ for each season. While the ranks of sending and receiving communities may differ, one cannot figure the difference within a single season. Therefore, if the ranks of neighboring seasons are the same, we assume a constant number of communities across seasons. If the minimal number of communities identified via scree plots differs between consecutive seasons, we assume that one possible scenario on the ranks along the seasons can be chosen. We will show the examples in Section 6.

Remark 3.3 The co-spectral clustering method in this approach relies on k -means clustering. However, community detection across different seasons may yield inconsistent labels. Even if most nodes remain in the same community, a shift in labeling can create interpretation issues. To address this, labels can be locally rearranged between consecutive detected groups to ensure consistency. Rearranging labels prevents unnecessary fluctuations in assigned labels without affecting fitting performance. Unlike the label-switching issue in other dynamic network models (e.g., Xu and Hero; 2014; Matias and Miele; 2017), where estimation is influenced by community detection, our re-labeling serves only to improve interpretability. It ensures that detected communities remain stable over time without affecting model identifiability.

4 Theoretical properties

In this section, we demonstrate the theoretical aspect of the ScBM-VAR-type models. The section is organized into three parts. First, we explain the stability condition of the ScBM-VAR-type models. Next, we show the consistency of the estimators combining two error sources. Finally, we delve into the algorithm’s performance.

Note that the proof strategy follows the two previous studies by Rohe et al. (2016) and Guðmundsson and Brownlees (2021). Both papers are rooted in the same seminar paper Rohe et al. (2011) so the theoretical arguments have quite similar flows. From the former reference, we investigate what has changed from a single network to a sequence of networks. Similarly, we emphasize the changes in proofs from a VAR-based undirected network to PVAR to VHAR-based directed multiple networks.

Regarding the theory of ScBM-VHAR, if the object of the theorem stems from time series models, VHAR can be regarded as a special case of the VAR model with longer lag order terms. Therefore, some of the proofs remain the same as the VAR case in Guðmundsson and Brownlees (2021). On the other hand, if the goal is to demonstrate the graph-related characteristics, ScBM-VHAR is considered a special case of ScBM-PVAR with $s = 3$.

4.1 Stability

4.1.1 Stability of ScBM-PVAR

To show that the ScBM-PVAR model (3) with (9) has a stable process, we follow the argument by Ursu and Duchesne (2009) and Boubacar Mainassara and Ursu (2023). We consider $T = Ns$ so that the observations exactly end at N th cycle of the season. Define $p^* = \lceil p/s \rceil$. Then the model (3) can be written as

$$\Phi_0^* Y_n^* = \sum_{h=1}^{p^*} \Phi_h^* Y_{n-h}^* + \varepsilon_n^*, \quad (19)$$

where $Y_n^* = (Y'_{s+ns}, Y'_{s-1+ns}, \dots, Y'_{1+ns})' \in \mathbb{R}^{qs}$, $\varepsilon_n^* = (\varepsilon'_{s+ns}, \varepsilon'_{s-1+ns}, \dots, \varepsilon'_{1+ns})' \in \mathbb{R}^{qs}$ and

$$\Phi_0^* = \begin{pmatrix} I_q & -\Phi_{1,s} & -\Phi_{2,s} & \dots & -\Phi_{s-2,s} & -\Phi_{s-1,s} \\ 0 & I_q & -\Phi_{1,s-1} & \dots & -\Phi_{s-3,s-1} & -\Phi_{s-2,s-1} \\ \vdots & \vdots & \vdots & \ddots & \vdots & \vdots \\ 0 & 0 & 0 & \dots & I_q & -\Phi_{1,2} \\ 0 & 0 & 0 & \dots & 0 & I_q \end{pmatrix} \quad (20)$$

and

$$\Phi_h^* = \begin{pmatrix} \Phi_{hs,s} & \Phi_{hs+1,s} & \dots & \Phi_{hs+s-1,s} \\ \Phi_{hs-1,s-1} & \Phi_{hs,s-1} & \dots & \Phi_{hs+s-2,s-1} \\ \vdots & \vdots & \ddots & \vdots \\ \Phi_{hs-s+1,1} & \Phi_{hs-s+2,1} & \dots & \Phi_{hs,1} \end{pmatrix}, \quad h = 1, \dots, p^*, \quad (21)$$

and take $\Phi_{\ell,m} = 0$, $\ell > p^*$, $m = 1, \dots, s$. Note that this construction is quite similar to the setup for stating the stability of structural VAR models (SVAR, e.g., Chapter 9 in Lütkepohl; 2005). Dividing both sides in (19) by Φ_0^* yields a VAR(p^*) model,

$$Y_n^* = \sum_{h=1}^{p^*} \underbrace{(\Phi_0^*)^{-1} \Phi_h^*}_{=\Psi_h^*} Y_{n-h}^* + \Phi_0^{*-1} \varepsilon_n^*, \quad (22)$$

To complete the statement of the stability, we impose the following assumption.

Assumption A.1 *We assume the following*

(i) *For all complex numbers z satisfying $|z| \leq 1$,*

$$\det(\Phi_0^* - \Phi_1^* z - \dots - \Phi_{p^*}^* z^{p^*}) \neq 0.$$

(ii) *Let $\phi(h) = \sum_{m=1}^s \phi_{hs,m}$, $h = 1, \dots, p^*$, where $\|\Phi_{hs,m}\| \leq \phi_{hs,m}$. Then*

$$\sum_{h=1}^{p^*} \phi(h) < 1$$

is satisfied. Here $\phi_{hs,m}$ have non-zero values when $hs \leq p^$ for each h .*

Note that the condition (i) is the common assumption for the stability of VAR-type models. In particular, if $p_m = 1$ for all m , this condition reduces to

$$\det(\Phi_0^* - \Phi_1^* z) = \det \left[I_q - \left(\prod_{m=1}^{s-1} \Phi_{1,s-m} \right) z \right] \neq 0$$

for all z such that $|z| \leq 1$. That is, the argument becomes equivalent to checking the stability of s different VAR(1) models (see Section 2.1 in Ursu and Duchesne; 2009). The condition (ii) is additionally imposed by the NAR models (e.g., Guðmundsson and Brownlees; 2021; Yin et al.; 2023) as constant to tune the entire scale of the transition matrices. Finally, if $s = 1$, then the model reduces to VAR model (1) with (8).

Lemma 4.1 *Suppose that (i) and (ii) in Assumption A.1 are satisfied. Then the ScBM-PVAR model (3) with (9) is stable.*

4.1.2 Stability of ScBM-VHAR

Next, we consider the ScBM-VHAR model (4) with (8). By following Baek and Park (2021), VHAR can be regarded as VAR(22) with restrictive transition matrices described in (6). Thus, Assumption A.3 changes to the following.

Assumption A.2 *We assume the following*

(i) *For all complex numbers z satisfying $|z| \leq 1$,*

$$\det \left(I_q - \left(\Phi_{(d)} + \frac{1}{5} \Phi_{(w)} + \frac{1}{22} \Phi_{(m)} \right) z - \sum_{h=2}^5 \left(\frac{1}{5} \Phi_{(w)} + \frac{1}{22} \Phi_{(m)} \right) z^h - \sum_{h=6}^{22} \frac{1}{22} \Phi_{(m)} z^h \right) \neq 0.$$

By using the restrictive coefficients in (6), this condition is equivalent to

$$\det \left(I_q - \sum_{h=1}^{22} \Phi_h z^h \right) \neq 0, \quad |z| \leq 1.$$

(ii) *Let $\phi_1 = \phi_{(d)} + \phi_{(w)}/5 + \phi_{(m)}/22$, $\phi_2 = \dots = \phi_5 = \phi_{(w)}/5 + \phi_{(m)}/22$, and $\phi_6 = \dots = \phi_{22} = \phi_{(m)}/22$. Then*

$$\sum_{h=1}^{22} \phi_h = \sum_{h \in \{d,w,m\}} \phi_{(h)} < 1$$

is satisfied.

We clarify the statement of the stability of the ScBM-VHAR models. The proof is analogous to the proof of Proposition 1 in Guðmundsson and Brownlees (2021) with $p = 22$. Therefore, we omit the proof of the following statement.

Corollary 4.1 *Suppose that (i) and (ii) in Assumption A.2 be satisfied. The the ScBM-VHAR model (4) with (10) is stable.*

4.2 Consistency

To establish the concentration bound of the estimation error of the autoregressive matrices, we divide the error into two parts based on the source of randomness. The first part is the errors caused by estimation with a finite sample size. The second part is due to the discrepancy between the population graph and its realization identifiable up to their rotational transform.

The key idea for showing the consistency of the estimators is that the ScBM-PVAR and ScBM-VHAR models can be described analogously to the ScBM-VAR model, which leads to follow a similar proof strategy in Guðmundsson and Brownlees (2021). Specifically, consider the ScBM-PVAR model (3) with (9). Then define the stacked autoregressive matrices Φ ,

$$\Phi = \begin{pmatrix} \Phi_1 \\ \vdots \\ \Phi_s \end{pmatrix} \in \mathbb{R}^{qs \times q}. \quad (23)$$

A similar construction can be made with the estimators $\{\hat{\Phi}_m\}_{m=1,\dots,s}$ and realized autoregressive matrices of population networks denoted by $\{\tilde{\Phi}_m\}_{m=1,\dots,s}$, identified up to their rotational transform, $m = 1, \dots, s$. If $s = 1$, this reduces to the decomposition of the case of ScBM-VAR (1) with (8), which is a directed network analog of Guðmundsson and Brownlees (2021). For the case of ScBM-VHAR model (4) with (10), we use $\Phi_{(d)}$, $\Phi_{(w)}$, and $\Phi_{(m)}$, and their sample and realized population analogues. That is, the ScBM-VHAR model can be viewed as a special case of the ScBM-PVAR model with $s = 3$. The estimation error of the stacked autoregressive matrices (23) can be decomposed as

$$\|\hat{\Phi} - \tilde{\Phi}\| \leq \|\hat{\Phi} - \Phi\| + \|\tilde{\Phi} - \Phi\|. \quad (24)$$

The following two subsections contribute to constructing upper bounds for the each of terms (24).

4.2.1 Error bound by finite samples

First, consider the case of ScBM-PVAR. For simplicity, assume that $T = Ns$ so that the series $Y_t = Y_{ns+m}$ in (3) exactly ends at N th cycle of the observation T . Define qs -dimensional vectors by stacking up Y_{ns+m} and ε_{ns+m} within each cycle as

$$Y_n^* = \begin{pmatrix} Y_{ns+s} \\ Y_{ns+s-1} \\ \vdots \\ Y_{ns+1} \end{pmatrix}, \quad \varepsilon_n^* = \begin{pmatrix} \varepsilon_{ns+s} \\ \varepsilon_{ns+s-1} \\ \vdots \\ \varepsilon_{ns+1} \end{pmatrix}, \quad n = 0, 1, \dots, N-1, \quad (25)$$

and their $qs \times qs$ -dimensional covariance matrices by

$$\Sigma_Y^* = \text{diag}(\Sigma_{1,Y^*}, \dots, \Sigma_{s,Y^*}), \quad \Sigma_\varepsilon^* = \text{diag}(\Sigma_{1,\varepsilon^*}, \dots, \Sigma_{s,\varepsilon^*}).$$

Note that by seeing the observations in a single cycle together, one can make the augmented observation $\{Y_n^*\}$ second-order stationary. Here, by following Guðmundsson and Brownlees (2021), define $\mathcal{F}_{-\infty}^n$ and $\mathcal{F}_{n+\ell}^\infty$ be σ -algebras generated by $\{(\Sigma_Y^*)^{-1/2}Y_u^* : u \leq n\}$ and $\{(\Sigma_Y^*)^{-1/2}Y_u^* : u \geq n + \ell\}$, respectively. Then strong mixing coefficients $\alpha_{Y^*}(\ell)$ are defined as

$$\alpha_{Y^*}(\ell) = \sup_{\substack{A \in \mathcal{F}_{-\infty}^n \\ B \in \mathcal{F}_{n+\ell}^\infty}} |\mathbb{P}(A \cap B) - \mathbb{P}(A)\mathbb{P}(B)|. \quad (26)$$

Assumption A.3 (Guðmundsson and Brownlees (2021)) *For the ScBM-PVAR model (3) with (9), we assume the following.*

(i) *The qs -dimensional process $(\varepsilon_n^*)_{n \in \mathbb{Z}}$ is ergodic and $\mathbb{E}[\varepsilon_n^*] = 0$, $\text{Var}(\varepsilon_n^*) = \Sigma_\varepsilon^*$ and $\text{Cov}(\varepsilon_n^*, \varepsilon_{n-\ell}^*) = 0$ for all $\ell \in \mathbb{Z}$ and $\ell \neq 0$.*

(ii) *Σ_ε^* satisfies $\|\Sigma_\varepsilon^*\| < C_1$, $\|(\Sigma_\varepsilon^*)^{-1}\| < C_2$ for $C_1, C_2 > 0$.*

(iv) *$\{(\Sigma_Y^*)^{-1/2}Y_n^*\}$ is strongly mixing with mixing coefficients satisfying $\alpha_{Y^*}(\ell) \leq e^{-c_1 \ell^{\gamma_1}}$ for any $\ell > 0$, where $\gamma_1, c_1 > 0$ are constants.*

(v) *For any vector v with $\|v\| = 1$ and for any $\delta > 0$,*

$$\mathbb{P}\left(\left|v'(\Sigma_Y^*)^{-1/2}Y_n^*\right| > \delta\right) \leq e^{1-(\delta/c_2)^{\gamma_2}}$$

for all n , where $\gamma_2, c_2 > 0$ are constants.

(vi) *$N = \Omega((qs)^{2/\gamma-1})$, where $1/\gamma = 1/\gamma_1 + 1/\gamma_2$ and $\gamma < 1$.*

The assumptions are from Guðmundsson and Brownlees (2021) to apply Lemma 3 therein. The idea for the ScBM-PVAR model (3) is that by stacking up $\{Y_{ns+s}\}$ as (26) makes the qs -dimensional $\{Y_n^*\}$ behaves as the typical VAR model. Therefore, the conditions (iii)-(iv) in Assumption A.3 completes the statement of the consistency part from the estimation error. Note also that the ergodicity assumption is added in the condition (i). This implies

$$\frac{1}{N} \sum_{n=0}^{N-1} \text{vec}(\varepsilon_{ns+m} X'_{n,m}) \xrightarrow{\text{a.s.}} \mathbb{E}[\text{vec}(\varepsilon_{ns+m} X'_{n,m})] = 0,$$

which is explicitly stated in the condition (i) in Assumption 3 of Guðmundsson and Brownlees (2021). The condition (ii) in Assumption A.3 is relatively stronger to Assumption (A3) in Boubacar Maïnassara and Ursu (2023); $\mathbb{E}\|\varepsilon_n^*\|^{4+2\kappa} < \infty$. However, we assume the strong mixing coefficient to $\{Y_n^*\}$ instead of $\{\varepsilon_n^*\}$. Imposing the condition to $\{\varepsilon_n^*\}$ makes the analysis of this model complicated. As an example, the covariance matrix of the noise $\{\varepsilon_n^*\}$ and variables $\{Y_n^*\}$ in the variance of the estimator of the model transition matrices $\{\Phi_{h,m}\}$ in (3) cannot be decomposed

unless we impose the i.i.d. assumption to $\{\varepsilon_n^*\}$, according to Theorem 3.1 in Boubacar Mainassara and Ursu (2023) (compare also to Theorem 3 in Ursu and Duchesne (2009)). Furthermore, strong mixing coefficient condition is often imposed to $\{Y_n^*\}$ in weak VARMA-type models (e.g., Francq et al.; 2005; Francq and Raïssi; 2007).

Lemma 4.2 *Suppose that (i)–(vi) in Assumptions A.3 are satisfied. Then for the stable ScBM-PVAR model (3) with (9),*

$$\|\hat{\Phi} - \Phi\| \leq \mathcal{O}\left(\sqrt{\frac{q}{N}}\right) \quad (27)$$

with high probability.

The case of the ScBM-VHAR model (4) can be viewed as a special case of the ScBM-PVAR model, where $s = 3$ and $p_m = 1$ for all $m = 1, 2, 3$.

Corollary 4.2 *Suppose that Assumption A.3 with $s = 3$ and $p_m = 1$ is satisfied. Then for the stable ScBM-VHAR model (4) with (10),*

$$\|\hat{\Phi} - \Phi\| \leq \mathcal{O}\left(\sqrt{\frac{q}{N}}\right) \quad (28)$$

with high probability, where $N = T - 22$.

Note that from Lemma 4.2 and Corollary (4.2), the upper bounds of the estimation error in the ScBM-PVAR and the ScBM-VHAR are slightly different. However, the form of the upper bounds of the estimation errors of both models is similar to that in Guðmundsson and Brownlees (2021).

4.2.2 Error bound by realized population graphs

To perform the clustering analysis on the graphs through either estimated or model transition matrices, we construct Laplacian matrices (e.g., Merris; 1994; Chung; 1997) to smooth the in- and out-degrees in the standardized adjacency matrices. Similar construction has been made in the algorithms described in Section 3. Similar to Assumption A2 in Guðmundsson and Brownlees (2021), we also assume the following.

Assumption A.4 *We assume that*

$$\delta + \tau = \Omega\left(\sum_{m=1}^s \min\left\{\sum_{i=1}^q [B_m]_{y_i z_j}, \sum_{j=1}^q [B_m]_{y_i z_j}\right\}\right) = \Omega(sq B_{sq}) \quad (29)$$

where $B_{sq} = \Omega(\log(sq)/(sq))$.

Assumption A.4 states the edge probabilities are reciprocal to the size of the graph q multiplied by the number of seasons s . The result is not surprising in that the q -dimensional PVAR model with season s can be viewed as a VAR model with the dimension of qs .

Lemma 4.3 Consider a stable ScBM-PVAR model (3) with (9) or ScBM-VHAR model (4) with (10). Then with Assumption (29),

$$\|\tilde{\Phi} - \Phi\| \leq \mathcal{O} \left(\sqrt{\frac{\log(sq)}{sqB_{sq}}} \right) \quad (30)$$

with a high probability.

4.2.3 Singular vectors

Finally, we prove the upper bound of the sum of differences between the population and empirical singular vectors. Define the stacked estimated left and right singular vectors, \hat{X}_L and \hat{X}_R , arranged by the formation of A used in the proof of Lemma 4.3. Then let their rowwise scaled singular vectors are defined by \hat{X}_L^* , \hat{X}_R^* . Similar to the estimator, the stacked singular left and right vectors from the population graph by \mathcal{X}_L^* , \mathcal{X}_R^* derived from \mathcal{A} , and their block matrices of orthogonal rotation maps \mathcal{R}_L and \mathcal{R}_R used for identifiability purpose.

Lemma 4.4 Consider ScBM-PVAR (3). Then

$$\|\hat{X}_L^* - \mathcal{X}_L^* \mathcal{R}_L\| + \|\hat{X}_R^* - \mathcal{X}_R^* \mathcal{R}_R\| = \mathcal{O} \left(\frac{sq}{\sqrt{T}} + \sqrt{\frac{\log(sq)}{B_{sq}}} \right), \quad (31)$$

with a high probability.

For the ScBM-VHAR (4), the upper bound rate is similar to the result derived in Lemma 4.4. Therefore, we state the following corollary without proof.

Corollary 4.3 Consider ScBM-VHAR (4). Then

$$\|\hat{X}_L^* - \mathcal{X}_L^* \mathcal{R}_L\| + \|\hat{X}_R^* - \mathcal{X}_R^* \mathcal{R}_R\| = \mathcal{O} \left(\frac{q}{\sqrt{N}} + \sqrt{\frac{\log(sq)}{B_{sq}}} \right), \quad (32)$$

with $s = 3, N = T - 22$ and the same high probability as Lemma 4.4.

4.3 Performance of the algorithm

The misclassification rates are an obvious metric to evaluate the performance of the algorithm. Since we smooth the singular vectors of the random graphs at each season and the propagating community structures are equivalent, the misclassification rate can be measured on average among the seasons. On the other hand, the convergence of the algorithm is obvious as we do not depart from the PisCES algorithm.

4.3.1 Misclassification rates

To consider the clustering for input Y_m , $m = 1, \dots, s$, by following Rohe et al. (2016), define the sets of nodes Y -misclutered at season m as

$$\mathcal{N}_m^y = \{i : \|[\hat{C}_{m,L}]_i - [C_{m,L}]_i\|_2 > \|[\hat{C}_{m,L}]_j - [C_{m,L}]_j\|_2 \text{ for any } i \neq j\},$$

where $\hat{C}_{m,L}$ is the estimated centroid matrix of the left singular vectors at season m and its population analog $C_{m,L}$. Similarly, for output Z_m , $m = 1, \dots, s$, define the set of nodes Z -misclustered at season m by

$$\mathcal{N}_m^z = \{i : \|[\hat{C}_{m,R}]_i - [C_{m,R}]_i\|_2 > \|[\hat{C}_{m,R}]_j - [C_{m,R}]_j\|_2 \text{ for any } i \neq j\},$$

where $\hat{C}_{m,R}$ is the estimated centroid matrix of the right singular vectors at season m and its population analog $C_{m,R}$.

Lemma 4.5 *Consider ScBM-PVAR (3). Then*

$$\frac{1}{s} \sum_{m=1}^s \frac{|\mathcal{N}_m^y|}{q} + \frac{1}{s} \sum_{m=1}^s \frac{|\mathcal{N}_m^z|}{q} \leq \mathcal{O} \left(\frac{sq}{T} + \frac{\log(sq)}{sqB_{sq}} \right). \quad (33)$$

with a high probability.

For the same reason used in Corollary 4.3, the upper bound rate of the ScBM-VHAR model (4) is obtained similarly. Therefore, we also state the following corollary without proof.

Corollary 4.4 *Consider ScBM-VHAR (4). Then*

$$\frac{1}{3} \sum_{m \in \{d, w, m\}} \frac{|\mathcal{N}_{(m)}^y|}{q} + \frac{1}{3} \sum_{m \in \{d, w, m\}} \frac{|\mathcal{N}_{(m)}^z|}{q} \leq \mathcal{O} \left(\frac{q}{T} + \frac{\log(sq)}{sqB_{sq}} \right). \quad (34)$$

with $s = 3, N = T - 22$ and the same high probability as Lemma 4.4.

4.3.2 Convergence of the algorithm

The following result is the consequence of Theorem 1 in Liu et al. (2018) by applying the PisCES algorithm to the Laplacian matrices from left and right singular vectors, separately. Therefore, with the α in the same range stated in the condition, each application becomes a contraction mapping. We state the theorem without the proof.

Lemma 4.6 (Theorem 1 in Liu et al. (2018)) *For $\alpha < \alpha_{\max} = \frac{1}{4\sqrt{2+2}}$, the algorithm converges to the global minimizer of the equations (add equation numbers) under any feasible initialization.*

5 Finite sample performances

5.1 Simulation design

In this section, we illustrate the finite-sample properties of the algorithm based on the ScBM-PVAR and ScBM-VHAR models through simulation. For the ScBM-PVAR model, we set $s = 4$ and fix the total number of communities at 5, with each community having equal size $q/5$. The number of effective communities, $K = K_m = K_{m_y} = K_{m_z}$, varies, where only the corresponding entries in B_m —the expected number of links between communities—are nonzero. For example, if $K = 2$, then only $[B_m]_{xy}$ for $x = 1, 2$ are nonzero for all seasons $m = 1, \dots, s$. We use $K = 2, 3, 5$ throughout the simulation.

Poisson sampling as discussed in Section (2) is applied. Consequently, increasing the number of effective communities does not necessarily make the transition matrices denser. Instead, it increases the number of distinct row patterns among nonzero rows, making the setting more challenging than simply increasing matrix density. The expected number of links between communities is set as $[B_m]_{xx} = 0.5$ for $x = 1, \dots, K$ and $[B_m]_{xx} = 0$ for $x = K + 1, \dots, 5$. To impose asymmetry, we vary the off-diagonal entries of B_m as $B_U = [B_m]_{xy}$ for $1 \leq x < y \leq K$ and $B_L = [B_m]_{xy}$ for $1 \leq y < x \leq K$ with all other entries set to 0.

The node degrees follow a log-normal distribution with a mean of 2 and a standard deviation of 1 on the log scale, matching the default setting in the R package `fastRG` by Rohe et al. (2018). To impose identifiability, we scale the sums within each community to one. Following Guðmundsson and Brownlees (2021), edge weights for nonzero entries are drawn from a uniform distribution on $[0.3, 1]$. Synthetic samples are generated with $q = 20, 30, 50, 100$ dimensions and sample sizes $T = 100, 200, 400, 1000, 2000, 4000$ for both time series models, using the transition matrices described above. The transition matrices are set with a constant $\phi_{m,h} = \phi_h = \phi = 0.99$ for all h and m . If the samples generated from the transition matrices and random graphs are unstable, meaning $\|\Phi\| > 0.95$ for the augmented matrix Φ when converting PVAR and VHAR to VAR(1), the constant is reduced by 0.1, and edges are resampled. The time series innovations follow a multivariate standard normal distribution for all seasons.

We use two performance metrics. First, clustering accuracy is measured by counting the number of estimated communities that match the actual communities. To account for all possible label permutations, we select the maximum accuracy. Without this adjustment, for example, if identified communities are labeled as 3 and 4 but correspond exactly to actual communities 1 and 2, the accuracy would incorrectly be considered zero. Clustering results are evaluated seasonally, but the final reported accuracy is the average across all seasons, computed similarly to (33) and (34). The ScBM-PVAR model yields identical accuracy for receiving and sending node communities, whereas the ScBM-VHAR model produces different accuracies for each. Second, we compute normalized

mutual information (NMI) (e.g., White and Liu; 1994; Vinh et al.; 2009; Gates and Ahn; 2017). Let \mathcal{C} denote the true community labels and $\hat{\mathcal{C}}$ the estimated labels at a fixed season $m = 1, \dots, s$, with $|\mathcal{C}| = |\hat{\mathcal{C}}| = K$. This setup includes clustering results for both sending and receiving communities. The NMI is defined as

$$\text{NMI}(\mathcal{C}, \hat{\mathcal{C}}) = \frac{2I(\mathcal{C}, \hat{\mathcal{C}})}{H(\mathcal{C}) + H(\hat{\mathcal{C}})},$$

where $I(\mathcal{C}, \hat{\mathcal{C}})$ is the mutual information between \mathcal{C} and $\hat{\mathcal{C}}$, and $H(\mathcal{C})$ is the entropy, given by

$$I(\mathcal{C}, \hat{\mathcal{C}}) = \sum_{i=1}^K \sum_{j=1}^K \frac{q_{i,j}}{q} \log \frac{q_{i,j}q}{q_i q_j}, \quad H(\mathcal{C}) = - \sum_{i=1}^K \frac{q_i}{q} \log \frac{q_i}{q}.$$

The entropy $H(\hat{\mathcal{C}})$ is defined similarly. NMI ranges from 0 to 1, approaching 1 when the clustering result closely matches the ground truth. It is also invariant to community size and robust to class imbalances (see Vinh et al.; 2009, for a related discussion).

5.2 Simulation result

Table 1 summarizes the clustering accuracy and NMI for ScBM-PVAR models under various values of q, T, K and the expected number of links between communities, $\{B_m\}_{m=1, \dots, s}$. Note that those metrics tend to be consistently higher when the number of variables q is smaller and the time series length T is larger. This pattern aligns with the characteristics of estimators in typical time series models. Both metrics decline as network connectivity becomes more complex; when there are more links between different communities generated. The number of effective communities K also influences these metrics. However, its impact is relatively marginal compared to the other factors.

Interestingly, the clustering accuracy remains higher than the results reported in Guðmundsson and Brownlees (2021), and its improvement with smaller q and larger T is relatively modest. We conjecture that while the upper bound of the misclassification rate is higher than in the VAR model with a symmetrized single network from Guðmundsson and Brownlees (2021), as seen from the result in Section 4, the lower bound might be relatively lower. It is inspiring that the clustering performance remains substantially strong, whereas the performance of their VAR model deteriorates sharply for higher lag orders p .

Table 2 presents the clustering analysis results for the ScBM-VHAR model. The performance, as measured by the evaluation metrics, closely resembles that of the ScBM-PVAR model. Based on the results from both models, we can construct dynamic networks that represent community trajectories evolving over seasons, whether these patterns are periodic or transient.

		T		100		200		400		1000		2000		4000	
K = 2	$b_D/b_U/b_L$	$q = 20$													
	0.5/0.05/0.1	0.786	0.203	0.795	0.23	0.801	0.238	0.815	0.248	0.817	0.243	0.817	0.236		
	0.5/0.15/0.1	0.787	0.206	0.791	0.222	0.796	0.237	0.804	0.239	0.807	0.237	0.805	0.231		
	0.5/0.25/0.1	0.787	0.208	0.793	0.224	0.800	0.242	0.801	0.236	0.805	0.237	0.805	0.230		
	$b_D/b_U/b_L$	$q = 30$													
	0.5/0.05/0.1	0.765	0.126	0.769	0.134	0.778	0.159	0.793	0.174	0.801	0.176	0.800	0.167		
	0.5/0.15/0.1	0.764	0.124	0.769	0.133	0.775	0.156	0.782	0.167	0.786	0.169	0.789	0.159		
	0.5/0.25/0.1	0.762	0.123	0.767	0.134	0.774	0.156	0.782	0.165	0.785	0.166	0.783	0.154		
	$b_D/b_U/b_L$	$q = 50$													
	0.5/0.05/0.1	0.748	0.067	0.741	0.057	0.750	0.075	0.768	0.113	0.780	0.119	0.796	0.123		
	0.5/0.15/0.1	0.747	0.068	0.749	0.072	0.748	0.074	0.764	0.111	0.768	0.112	0.775	0.108		
	0.5/0.25/0.1	0.746	0.067	0.750	0.064	0.748	0.074	0.763	0.111	0.766	0.112	0.770	0.106		
	$b_D/b_U/b_L$	$q = 100$													
	0.5/0.05/0.1	0.729	0.031	0.728	0.028	0.730	0.027	0.734	0.039	0.752	0.076	0.768	0.086		
	0.5/0.15/0.1	0.728	0.029	0.728	0.029	0.722	0.027	0.734	0.038	0.747	0.075	0.753	0.084		
0.5/0.25/0.1	0.728	0.030	0.727	0.028	0.726	0.026	0.733	0.039	0.747	0.076	0.751	0.082			
K = 3	$b_D/b_U/b_L$	$q = 20$													
	0.5/0.05/0.1	0.779	0.199	0.793	0.238	0.793	0.238	0.808	0.252	0.817	0.268	0.819	0.259		
	0.4/0.15/0.15	0.781	0.200	0.781	0.216	0.786	0.230	0.792	0.231	0.798	0.237	0.804	0.235		
	0.5/0.25/0.1	0.778	0.195	0.782	0.218	0.787	0.226	0.790	0.228	0.793	0.227	0.799	0.229		
	$b_D/b_U/b_L$	$q = 30$													
	0.5/0.05/0.1	0.763	0.124	0.762	0.126	0.768	0.149	0.782	0.168	0.799	0.192	0.809	0.199		
	0.5/0.15/0.1	0.764	0.128	0.764	0.129	0.764	0.143	0.769	0.152	0.778	0.158	0.782	0.164		
	0.5/0.25/0.1	0.765	0.127	0.764	0.129	0.762	0.141	0.769	0.152	0.772	0.154	0.779	0.159		
	$b_D/b_U/b_L$	$q = 50$													
	0.5/0.05/0.1	0.744	0.066	0.744	0.060	0.746	0.072	0.752	0.096	0.767	0.108	0.790	0.134		
	0.5/0.15/0.1	0.745	0.067	0.740	0.062	0.745	0.072	0.747	0.091	0.753	0.095	0.762	0.103		
	0.5/0.25/0.1	0.746	0.069	0.742	0.065	0.745	0.072	0.747	0.090	0.752	0.094	0.756	0.093		
	$b_D/b_U/b_L$	$q = 100$													
	0.5/0.05/0.1	0.726	0.030	0.727	0.029	0.723	0.028	0.726	0.036	0.732	0.050	0.746	0.061		
	0.5/0.15/0.1	0.725	0.029	0.726	0.029	0.725	0.028	0.727	0.035	0.729	0.047	0.733	0.051		
0.5/0.25/0.1	0.726	0.029	0.726	0.029	0.728	0.028	0.727	0.035	0.728	0.046	0.731	0.050			
K = 5	$b_D/b_U/b_L$	$q = 20$													
	0.5/0.05/0.1	0.773	0.197	0.775	0.202	0.778	0.210	0.781	0.220	0.792	0.245	0.807	0.282		
	0.5/0.15/0.1	0.770	0.192	0.771	0.198	0.774	0.201	0.778	0.208	0.781	0.216	0.785	0.228		
	0.5/0.25/0.1	0.774	0.200	0.774	0.201	0.775	0.203	0.777	0.205	0.781	0.217	0.783	0.224		
	$b_D/b_U/b_L$	$q = 30$													
	0.5/0.05/0.1	0.755	0.123	0.754	0.121	0.757	0.127	0.762	0.136	0.770	0.155	0.781	0.185		
	0.5/0.15/0.1	0.755	0.121	0.754	0.121	0.756	0.125	0.759	0.130	0.760	0.133	0.767	0.151		
	0.5/0.25/0.1	0.755	0.125	0.753	0.121	0.754	0.124	0.756	0.125	0.759	0.130	0.762	0.139		
	$b_D/b_U/b_L$	$q = 50$													
	0.5/0.05/0.1	0.737	0.067	0.730	0.057	0.737	0.066	0.739	0.071	0.742	0.075	0.751	0.092		
	0.5/0.15/0.1	0.737	0.066	0.742	0.069	0.736	0.065	0.738	0.068	0.739	0.070	0.743	0.077		
	0.5/0.25/0.1	0.736	0.065	0.738	0.066	0.737	0.064	0.737	0.065	0.737	0.067	0.741	0.073		
	$b_D/b_U/b_L$	$q = 100$													
	0.5/0.05/0.1	0.719	0.027	0.719	0.028	0.718	0.028	0.720	0.029	0.721	0.03	0.724	0.035		
	0.5/0.15/0.1	0.719	0.028	0.719	0.028	0.714	0.023	0.719	0.027	0.720	0.029	0.721	0.031		
0.5/0.25/0.1	0.719	0.028	0.719	0.027	0.719	0.027	0.719	0.028	0.720	0.029	0.721	0.030			

Table 1: Table for accuracy and NMI from ScBM-PVAR models (3) with (9) along with various number of nodes, sample lengths, number of effective communities, and r community link matrices. One value for each setting is reported since the results for sending and receiving communities are identical.

		T		100		200		400		1000		2000		4000	
K = 2	$b_D/b_U/b_L$	q = 20													
	0.5/0.05/0.1	0.785	0.201	0.793	0.215	0.799	0.228	0.808	0.236	0.814	0.241	0.816	0.235		
	0.5/0.15/0.1	0.785	0.199	0.789	0.211	0.793	0.221	0.800	0.232	0.801	0.230	0.804	0.233		
	0.5/0.25/0.1	0.784	0.202	0.789	0.216	0.794	0.224	0.800	0.231	0.804	0.237	0.802	0.229		
	$b_D/b_U/b_L$	q = 30													
	0.5/0.05/0.1	0.764	0.123	0.766	0.125	0.776	0.139	0.786	0.161	0.791	0.163	0.797	0.167		
	0.5/0.15/0.1	0.764	0.126	0.764	0.124	0.772	0.138	0.779	0.151	0.788	0.161	0.788	0.166		
	0.5/0.25/0.1	0.768	0.125	0.763	0.130	0.774	0.142	0.776	0.152	0.785	0.156	0.784	0.162		
	$b_D/b_U/b_L$	q = 50													
	0.5/0.05/0.1	0.747	0.065	0.746	0.065	0.753	0.076	0.759	0.086	0.772	0.106	0.779	0.108		
	0.5/0.15/0.1	0.745	0.065	0.749	0.065	0.749	0.075	0.757	0.086	0.768	0.102	0.767	0.100		
	0.5/0.25/0.1	0.745	0.065	0.746	0.065	0.752	0.076	0.757	0.084	0.763	0.096	0.769	0.101		
	$b_D/b_U/b_L$	q = 100													
	0.5/0.05/0.1	0.729	0.028	0.727	0.028	0.728	0.029	0.734	0.039	0.742	0.046	0.759	0.063		
	0.5/0.15/0.1	0.728	0.028	0.726	0.029	0.728	0.028	0.733	0.039	0.738	0.043	0.749	0.058		
0.5/0.25/0.1	0.729	0.028	0.728	0.029	0.728	0.028	0.734	0.039	0.734	0.042	0.743	0.056			
K = 3	$b_D/b_U/b_L$	q = 20													
	0.5/0.05/0.1	0.784	0.203	0.782	0.208	0.787	0.216	0.796	0.231	0.803	0.241	0.806	0.246		
	0.5/0.15/0.15	0.783	0.199	0.784	0.206	0.785	0.213	0.790	0.234	0.797	0.237	0.796	0.231		
	0.5/0.25/0.1	0.787	0.203	0.784	0.201	0.784	0.208	0.787	0.222	0.795	0.237	0.793	0.230		
	$b_D/b_U/b_L$	q = 30													
	0.5/0.05/0.1	0.763	0.123	0.753	0.120	0.766	0.133	0.771	0.148	0.780	0.161	0.790	0.180		
	0.5/0.15/0.1	0.764	0.124	0.753	0.119	0.762	0.130	0.767	0.147	0.771	0.150	0.775	0.160		
	0.5/0.25/0.1	0.761	0.121	0.754	0.122	0.763	0.131	0.766	0.143	0.768	0.147	0.774	0.154		
	$b_D/b_U/b_L$	q = 50													
	0.5/0.05/0.1	0.742	0.063	0.744	0.065	0.744	0.068	0.750	0.078	0.758	0.096	0.772	0.112		
	0.5/0.15/0.1	0.743	0.065	0.744	0.064	0.746	0.068	0.746	0.075	0.752	0.085	0.756	0.095		
	0.5/0.25/0.1	0.744	0.064	0.745	0.066	0.745	0.070	0.744	0.077	0.748	0.085	0.752	0.090		
	$b_D/b_U/b_L$	q = 100													
	0.5/0.05/0.1	0.726	0.029	0.725	0.028	0.726	0.029	0.726	0.033	0.729	0.038	0.738	0.048		
	0.5/0.15/0.1	0.726	0.029	0.726	0.029	0.727	0.029	0.727	0.033	0.728	0.035	0.730	0.040		
0.5/0.25/0.1	0.726	0.028	0.727	0.028	0.726	0.028	0.727	0.033	0.727	0.035	0.730	0.041			
K = 5	$b_D/b_U/b_L$	q = 20													
	0.5/0.05/0.1	0.775	0.204	0.775	0.202	0.777	0.208	0.782	0.217	0.785	0.226	0.795	0.251		
	0.5/0.15/0.1	0.772	0.198	0.774	0.201	0.774	0.201	0.776	0.204	0.780	0.214	0.781	0.218		
	0.5/0.25/0.1	0.773	0.198	0.776	0.204	0.773	0.201	0.774	0.202	0.777	0.212	0.779	0.212		
	$b_D/b_U/b_L$	q = 30													
	0.5/0.05/0.1	0.756	0.123	0.776	0.139	0.755	0.126	0.759	0.131	0.762	0.142	0.774	0.163		
	0.5/0.15/0.1	0.756	0.123	0.772	0.138	0.754	0.122	0.758	0.128	0.758	0.131	0.761	0.139		
	0.5/0.25/0.1	0.753	0.122	0.774	0.142	0.754	0.121	0.758	0.128	0.758	0.131	0.761	0.137		
	$b_D/b_U/b_L$	q = 50													
	0.5/0.05/0.1	0.737	0.066	0.735	0.060	0.737	0.066	0.739	0.069	0.742	0.073	0.746	0.084		
	0.5/0.15/0.1	0.737	0.065	0.736	0.063	0.737	0.064	0.738	0.067	0.738	0.069	0.739	0.072		
	0.5/0.25/0.1	0.737	0.066	0.738	0.065	0.737	0.066	0.738	0.068	0.739	0.069	0.739	0.070		
	$b_D/b_U/b_L$	q = 100													
	0.5/0.05/0.1	0.719	0.028	0.719	0.028	0.719	0.028	0.720	0.029	0.720	0.031	0.723	0.033		
	0.5/0.15/0.1	0.720	0.028	0.719	0.028	0.720	0.028	0.719	0.027	0.720	0.029	0.721	0.030		
0.5/0.25/0.1	0.719	0.028	0.719	0.028	0.719	0.027	0.719	0.028	0.720	0.029	0.721	0.030			

Table 2: Table for accuracy and NMI from ScBM-VHAR models (4) with (10) along with various number of nodes, sample lengths, number of effective communities, and r community link matrices.

6 Data applications

6.1 Quarterly employees on nonfarm payrolls by industry sectors

The number of employees on nonfarm payrolls by industry sector measures paid U.S. workers across selected industries, excluding farmworkers, private household employees, and military personnel. This data has been reported monthly by the U.S. Bureau of Labor Statistics, with industry categories available on its webpage*. The observations are also available in the Federal Reserve Economic Data†. We use quarterly observations by aggregating data every three months from January 1, 1990, to March 1, 2020, before the COVID-19 pandemic. The first observation date corresponds to the earliest availability of data for all sectors of interest. Since the largest sector categories alone do not constitute a high-dimensional time series, and periodic cyclic behaviors are not well observed, we include third- and fourth-level subcategories for some of the largest or second-largest sectors. The selected categories are summarized in Table C1 in Appendix B. In what follows, we use the table’s codes to refer to the sectors.

We applied log transformation and differencing to the quarterly aggregated data before fitting the model. Figure C1 in Appendix B presents time plots for the first eight time series, ordered according to Table C1, along with sample ACF plots for Mining, Nonduration, Wholesale, and Retail, and sample PACF plots for the same sectors. From the diagnostic plots, the sample ACF exhibits strong cyclic variations, while significant sample PACF values at higher lags are sparse. This suggests that periodic time series modeling is appropriate. Interestingly, while sample CCF indicates strong associations between employment in different sectors, not all time series within the same category follow the same patterns. For instance, the crash around 2008 Subprime Mortgage crisis (the time point around 80) is evident in most sections of the Manufacturing and Trade, Transportation, and Utilities categories, yet the Utility sector follows a different trajectory. Similarly, employment patterns in the Production category differ from those in Mining and Construction, where the crash around 1980 is either less pronounced or absent. These observations highlight the necessity of clustering analysis.

Figure C2 in Appendix B presents scree plots of the singular values from the estimated transition matrices of the ScBM-PVAR model considering four seasons ($s = 4$). For each season, the smallest number of singular values whose cumulative proportion of explained variation (blue dotted lines) exceeds the 70% threshold (black dotted line) is 2, 3, 4, and 2, respectively. Following Remark 3.2, this result implies $K_1 = \min(K_{1_y}, K_{1_z}) = 2$, $K_2 = \min(K_{2_y}, K_{2_z}) = 3$, $K_3 = \min(K_{3_y}, K_{3_z}) = 4$, and $K_4 = \min(K_{4_y}, K_{4_z}) = 2$. To incorporate the cyclic community structure over seasons, as described in Section 3.2, we impose $K_{1_z} = K_{2_y}$, $K_{2_z} = K_{3_y}$, $K_{3_z} = K_{4_y}$, and $K_{4_z} = K_{1_y}$. Thus,

*See <https://www.bls.gov/news.release/empsit.t17.htm>

†See <https://fred.stlouisfed.org/>

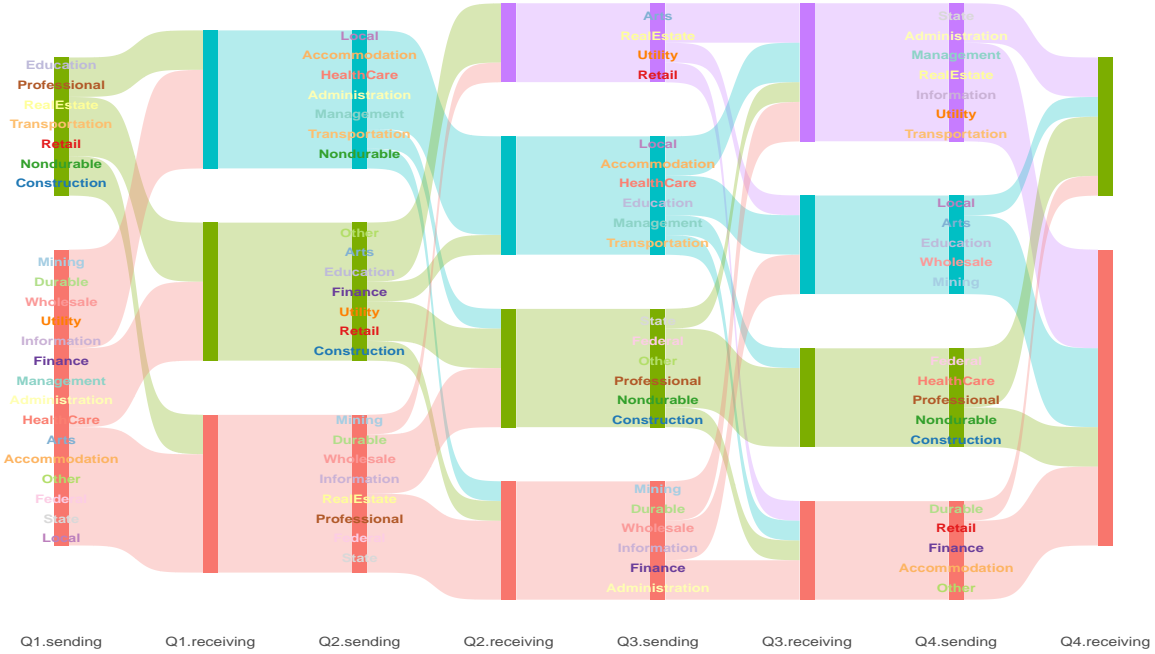


Figure 1: Cyclic evolution of 22 industry sectors in U.S. nonfarm payroll employment over four seasons (quarterly). Each pair of consecutive columns represents the community structure of one season. Sector codes are uniquely colored by state, while distinct communities are represented by different path colors. Community shifts occur at each season, but the structure between consecutive seasons remains unchanged. The flow width is proportional to the number of entries in each community.

one possible community configuration over the seasons is

$$(K_{1y}, K_{1z}, K_{2y}, K_{2z}, K_{3y}, K_{3z}, K_{4y}, K_{4z}) = (2, 3, 3, 4, 4, 4, 4, 3).$$

Figure 1 presents the constructed dynamic network from spectral clustering over four seasons, with transitions smoothed using the PisCES algorithm. Community labels for receiving nodes are omitted as they match those of sending nodes. Overall, cluster sizes remain evenly distributed across seasons, and community labels are relatively stable. Next, we trace the communities of selected sectors used in the sample ACF and PACF plots in Figure C1. For example, Mining consistently clusters with Wholesale in all seasons and with Durable in three seasons, while remaining separate from Nondurables and Retail throughout. Surprisingly, these results contrast with visual inspection, as it is unclear which of these three sectors exhibit patterns similar to Mining.

To track whether individual sectors have remained in the same communities, Figure 2 presents a discrepancy matrix summarizing how often each sector belongs to different communities from its corresponding sectors across all seasons. For example, this heatmap can be used to verify the case of Mining. Notably, some sectors within the same subcategories tend to cluster together, such as

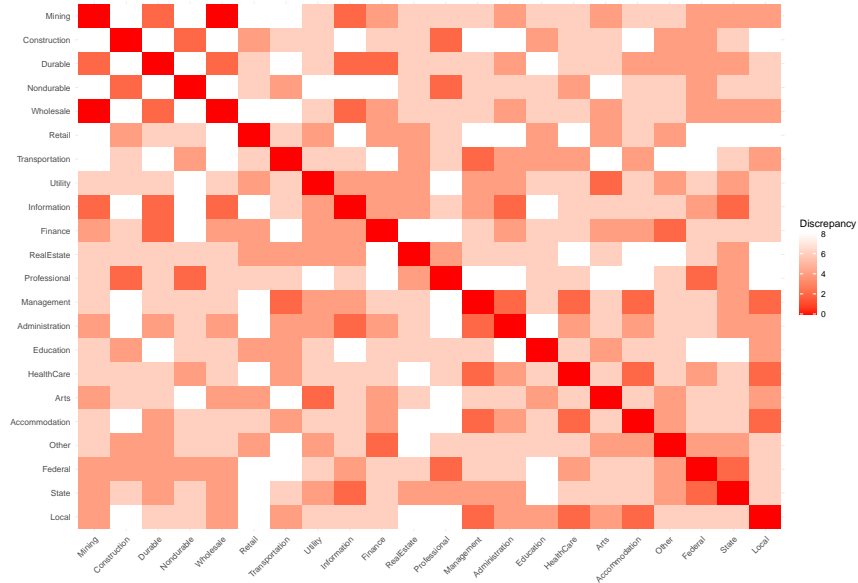


Figure 2: Discrepancy matrix for 22 industry sectors in nonfarm payroll employment, computed as the sum of counts indicating whether sectors belong to the same receiving and sending communities across all four seasons.

Federal, State, and Local in the Government category; Retail and Utility in Trade, Transportation, and Utilities; and Management and Administration in Professional and Business Services. However, this pattern does not always hold—for instance, Durable and Nondurable in Manufacturing belong to different communities. Further investigation into the clustering rationale is required for economic interpretation, which is beyond the scope of this study.

6.2 Realized volatilities of stock indices across different financial markets

Realized volatility (RV) is an ex-post measure of price variability for financial assets over a given historical period. It is typically computed as the square root of the sum of squared intraday returns, with 5-minute intraday returns aggregated in this study. We follow the data processing steps in Section 4.3 of Corsi (2009). RV quantifies historical price fluctuations, making it a valuable tool for risk assessment and volatility forecasting (e.g., Andersen et al.; 2003). This study considers 20 multinational RVs. The original data was previously provided by the Oxford-Man Institute of Quantitative Finance*, but is no longer available. Instead, we use the processed data from Baek and Park (2021). The market regions, continents, MSCI market classification (MSCI; 2025), and corresponding ticker symbols of the indices are summarized in Table C2 in Appendix B.

Figure C3 in Appendix B presents time plots of four selected stock indices (FTSE 100, Nikkei 225, KOSPI Composite Index, and IPC Mexico), along with their sample ACF and PACF plots.

*<http://realized.oxford-man.ox.ac.uk>

As seen in the bottom left panel, both ACFs and PACFs exhibit long-memory dependence, with significant CCFs persisting across long lag orders. Interestingly, not all indices display identical upward spikes and downward crashes. For instance, FTSE 100, KOSPI Composite Index, and IPC Mexico show sharp increases around time point 400 (approximately 1st quarter of 2011), whereas the Nikkei 225 exhibits a more gradual rise, peaking earlier. Furthermore, the KOSPI Composite Index appears more similar to the FTSE 100 than to the Nikkei 225, based on visual inspection. This suggests that stock index patterns are not necessarily influenced by geographical proximity, as indices from the same continent do not always follow similar trends. Identifying latent group structures can reveal deeper relationships beyond initial observations.

Figure C4 in Appendix B displays scree plots of singular values from the estimated transition matrices of the ScBM-VHAR model (4) with (10). By identifying the smallest number of singular values whose cumulative explained variation exceeds the threshold, we obtain $K_{(d)} = 3, K_{(w)} = 4, K_{(m)} = 3$. This sets the number of communities as $\min(K_{(d)_y}, K_{(d)_z}) = 3, \min(K_{(w)_y}, K_{(w)_z}) = 4$, and $\min(K_{(m)_y}, K_{(m)_z}) = 3$. Additionally, we impose the conditions $K_{(d)_z} = K_{(w)_y}$ and $K_{(w)_z} = K_{(m)_y}$. Thus, the selected community configuration is

$$(K_{(d)_y}, K_{(d)_z}, K_{(w)_y}, K_{(w)_z}, K_{(m)_y}, K_{(m)_z}) = (3, 4, 4, 4, 4, 3).$$

Figure 3 presents the constructed dynamic network from spectral clustering, capturing short-, medium-, and long-term effects of variation, with transitions smoothed using the PisCES algorithm. Unlike the previous example, the first and last communities do not necessarily share the same structures. To account for this, we adjust the discrepancy matrix by summing counts separately for each time horizon rather than across all seasons, providing more detailed insights. The resulting matrix is shown in Figure 4. Notably, community structures differ significantly across these three time horizons. For instance, the emerging market indices NSEI, MXX, and BVSP belong to different communities in the short- and medium-term effects but converge in the long-term effects. Meanwhile, FTSE, GDAXI, and FCHI cluster together in the short term but gradually diverge into separate communities over longer horizons. Understanding the rationale behind these structures would require macroeconomic interpretation, which is beyond the scope of this study.

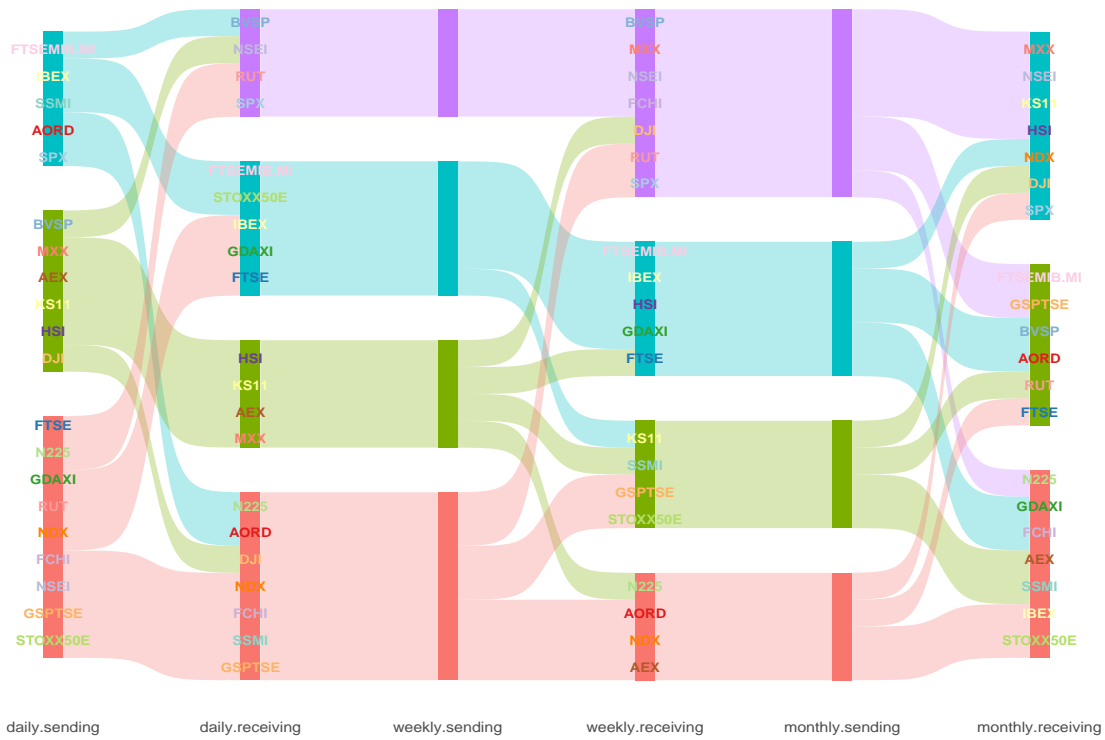


Figure 3: Progression of community structure in daily, weekly, and monthly realized volatilities of stock indices across 20 financial markets. Each pair of consecutive columns represents the daily, weekly, and monthly community structures. Abbreviation colors are unique to each state, while path colors indicate distinct communities. Community shifts occur at daily, weekly, and monthly cycles, with structures remaining unchanged between consecutive cycles. The flow width is proportional to the number of entries in each community.

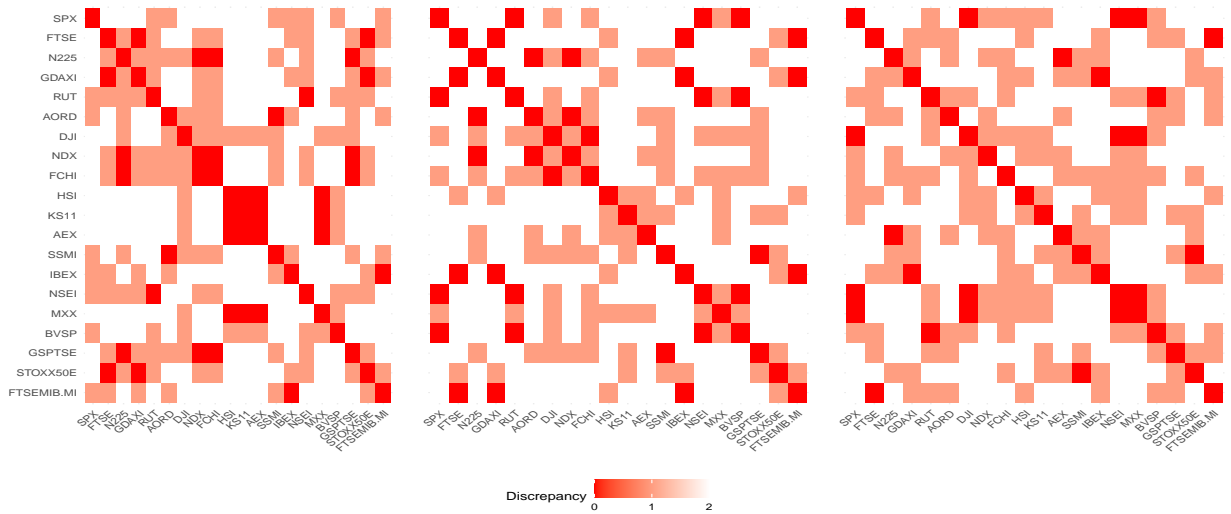


Figure 4: Discrepancy matrix for 20 realized volatilities of stock indices across 20 financial markets, computed as the sum of counts indicating whether indices belong to the same receiving and sending communities for short-, medium-, and long-term effects, respectively.

7 Conclusion

In this study, we proposed a dynamic network construction based on samples following one of two VAR-type models: PVAR and VHAR. The sequence of networks across seasons captures changes in community structure over time, enabling the tracking of network Granger causality paths. For each season, degree-corrected stochastic co-block models were used to represent directional connectivity between variable pairs, with network evolution controlled through a smoothing technique. We provided mathematical justification, demonstrating alignment with previous studies, and conducted extensive simulations to validate theoretical upper bounds on misclassification rates.

Applications to seasonal variations in nonfarm payroll employment and long-range dependence in global stock indices highlighted the method’s ability to reveal hidden community structures evolving over time. The R code for the simulation study in Section 5 and Appendix ??, as well as the two data applications in Section 6 and Appendix B, is available on GitHub at <https://github.com/yk748/ScBM-VAR>.

Despite its strengths, our approach has several limitations. First, determining the number of sending and receiving communities for each season is not straightforward. While we used scree plots and assumed an equal number of communities between consecutive seasons, this assumption was restrictive in real data analyses. Second, selecting lag orders for each season in the ScBM-PVAR model remains challenging. Even for simple PVAR models, identifying the optimal lag order is nontrivial. Lastly, our approach lacks a systematic method for tracking individual community evolution across seasons. Future advancements in dynamic network models may provide improved solutions.

Acknowledgement

CB was supported by National Research Foundation of Korea, NRF-2022R1F1A1066209.

References

- Andersen, T. G., Bollerslev, T., Diebold, F. X. and Labys, P. (2003), ‘Modeling and forecasting realized volatility’, *Econometrica* **71**(2), 579–625.
- Ando, T. and Bai, J. (2016), ‘Panel data models with grouped factor structure under unknown group membership’, *Journal of Applied Econometrics* **31**(1), 163–191.
- Ando, T. and Bai, J. (2017), ‘Clustering huge number of financial time series: A panel data approach with high-dimensional predictors and factor structures’, *Journal of the American Statistical Association* **112**(519), 1182–1198.
- Baek, C., Davis, R. A. and Pipiras, V. (2017), ‘Sparse seasonal and periodic vector autoregressive modeling’, *Computational Statistics & Data Analysis* **106**, 103–126.
- Baek, C., Davis, R. A. and Pipiras, V. (2018), ‘Periodic dynamic factor models: Estimation approaches and applications’, *Electronic Journal of Statistics* **12**, 4377–4411.
- Baek, C. and Park, M. (2021), ‘Sparse vector heterogeneous autoregressive modeling for realized volatility’, *Journal of the Korean Statistical Society* **50**, 495–510.

- Barigozzi, M., Cho, H. and Owens, D. (2023), ‘FNETS: factor-adjusted network estimation and forecasting for high-dimensional time series’, *Journal of Business & Economic Statistics* pp. 1–13.
- Basu, S. and Michailidis, G. (2015), ‘Regularized estimation in sparse high-dimensional time series models’, *The Annals of Statistics* **43**(4), 1535.
- Boubacar Maïnassara, Y. and Ursu, E. (2023), ‘Estimating weak periodic vector autoregressive time series’, *Test* **32**(3), 958–997.
- Brownlees, C., Guðmundsson, G. S. and Lugosi, G. (2022), ‘Community detection in partial correlation network models’, *Journal of Business & Economic Statistics* **40**(1), 216–226.
- Brownlees, C., Nualart, E. and Sun, Y. (2018), ‘Realized networks’, *Journal of Applied Econometrics* **33**(7), 986–1006.
- Chaudhuri, K., Chung, F. and Tsiatas, A. (2012), ‘Spectral clustering of graphs with general degrees in the extended planted partition model’, *Journal of Machine Learning Research* pp. 1–23.
- Chen, E. Y., Fan, J. and Zhu, X. (2022), ‘Community network auto-regression for high-dimensional time series’, *Journal of Econometrics* .
- Chung, F. R. (1997), *Spectral graph theory*, Vol. 92, American Mathematical Soc.
- Clements, A. and Preve, D. P. (2021), ‘A practical guide to harnessing the HAR volatility model’, *Journal of Banking & Finance* **133**, 106285.
- Corsi, F. (2009), ‘A simple approximate long-memory model of realized volatility’, *Journal of Financial Econometrics* **7**(2), 174–196.
- Cubadda, G., Guardabascio, B. and Hecq, A. (2017), ‘A vector heterogeneous autoregressive index model for realized volatility measures’, *International Journal of Forecasting* **33**(2), 337–344.
- Eichler, M. (2007), ‘Granger causality and path diagrams for multivariate time series’, *Journal of Econometrics* **137**(2), 334–353.
- Francq, C. and Raïssi, H. (2007), ‘Multivariate portmanteau test for autoregressive models with uncorrelated but nonindependent errors’, *Journal of Time Series Analysis* **28**(3), 454–470.
- Francq, C., Roy, R. and Zakoïan, J.-M. (2005), ‘Diagnostic checking in ARMA models with uncorrelated errors’, *Journal of the American Statistical Association* **100**(470), 532–544.
- Gates, A. J. and Ahn, Y.-Y. (2017), ‘The impact of random models on clustering similarity’, *Journal of Machine Learning Research* **18**(87), 1–28.
- Granger, C. W. (1969), ‘Investigating causal relations by econometric models and cross-spectral methods’, *Econometrica* pp. 424–438.
- Guðmundsson, G. S. and Brownlees, C. (2021), ‘Detecting groups in large vector autoregressions’, *Journal of Econometrics* **225**(1), 2–26.
- Hayashi, F. (2011), *Econometrics*, Princeton University Press.
- Holland, P. W., Laskey, K. B. and Leinhardt, S. (1983), ‘Stochastic blockmodels: First steps’, *Social Networks* **5**(2), 109–137.
- Horn, R. A. and Johnson, C. R. (2012), *Matrix Analysis*, Cambridge University Press.
- Ji, P., Jin, J., Ke, Z. T. and Li, W. (2022), ‘Co-citation and co-authorship networks of statisticians’, *Journal of Business & Economic Statistics* **40**(2), 469–485.
- Karrer, B. and Newman, M. E. (2011), ‘Stochastic blockmodels and community structure in networks’, *Physical Review E* **83**(1), 016107.
- Knight, M., Leeming, K., Nason, G. and Nunes, M. (2019), ‘Generalised network autoregressive processes and the GNAR package’, *arXiv preprint arXiv:1912.04758* .
- Kock, A. B. and Callot, L. (2015), ‘Oracle inequalities for high dimensional vector autoregressions’, *Journal of Econometrics* **186**(2), 325–344.
- Kolaczyk, E. D. (2009), *Statistical Analysis of Network Data: Methods and Models*, Springer Science & Business Media.
- Krampe, J. (2019), ‘Time series modeling on dynamic networks’, *Electronic Journal of Statistics* **13**(2), 4945–4976.
- Lei, J., Chen, K. and Lynch, B. (2020), ‘Consistent community detection in multi-layer network data’, *Biometrika* **107**(1), 61–73.
- Li, T., Levina, E. and Zhu, J. (2020), ‘Network cross-validation by edge sampling’, *Biometrika* **107**(2), 257–276.
- Liu, F., Choi, D., Xie, L. and Roeder, K. (2018), ‘Global spectral clustering in dynamic networks’, *Proceedings of the National Academy of Sciences* **115**(5), 927–932.

- Lütkepohl, H. (2005), *New Introduction to Multiple Time Series Analysis*, Springer Science & Business Media.
- Mantziou, A., Cucuringu, M., Meirinhos, V. and Reinert, G. (2023), ‘The GNAR-edge model: A network autoregressive model for networks with time-varying edge weights’, *arXiv preprint arXiv:2305.16097*.
- Martin, B., Passino, F. S., Cucuringu, M. and Luati, A. (2024), ‘NIRVAR: Network informed restricted vector autoregression’, *arXiv preprint arXiv:2407.13314*.
- Matias, C. and Miele, V. (2017), ‘Statistical clustering of temporal networks through a dynamic stochastic block model’, *Journal of the Royal Statistical Society. Series B (Statistical Methodology)* **79**(4), 1119–1141.
- Merris, R. (1994), ‘Laplacian matrices of graphs: a survey’, *Linear Algebra and its Applications* **197**, 143–176.
- MSCI (2025), ‘GICS: global industry classification standard’. Accessed: 8 January 2025.
URL: <https://www.msci.com/our-solutions/indices/gics>
- Qin, T. and Rohe, K. (2013), ‘Regularized spectral clustering under the degree-corrected stochastic blockmodel’, *Advances in Neural Information Processing Systems* **26**.
- Rohe, K., Chatterjee, S. and Yu, B. (2011), ‘Spectral clustering and the high-dimensional stochastic blockmodel’, *The Annals of Statistics* **39**(4), 1878–1915.
- Rohe, K., Qin, T. and Yu, B. (2016), ‘Co-clustering directed graphs to discover asymmetries and directional communities’, *Proceedings of the National Academy of Sciences* **113**(45), 12679–12684.
- Rohe, K., Tao, J., Han, X. and Binkiewicz, N. (2018), ‘A note on quickly sampling a sparse matrix with low rank expectation’, *Journal of Machine Learning Research* **19**(77), 1–13.
- Salas, H. N. (1999), ‘Gershgorin’s theorem for matrices of operators’, *Linear Algebra and its Applications* **291**(1-3), 15–36.
- Schönemann, P. H. (1966), ‘A generalized solution of the orthogonal Procrustes problem’, *Psychometrika* **31**(1), 1–10.
- Shen, H. and Huang, J. Z. (2008), ‘Sparse principal component analysis via regularized low rank matrix approximation’, *Journal of Multivariate Analysis* **99**(6), 1015–1034.
- Shojaie, A. and Fox, E. B. (2022), ‘Granger causality: A review and recent advances’, *Annual Review of Statistics and Its Application* **9**, 289–319.
- Ursu, E. and Duchesne, P. (2009), ‘On modelling and diagnostic checking of vector periodic autoregressive time series models’, *Journal of Time Series Analysis* **30**(1), 70–96.
- Vershynin, R. (2018), *High-Dimensional Probability: An Introduction with Applications in Data Science*, Vol. 47, Cambridge University Press.
- Vinh, N. X., Epps, J. and Bailey, J. (2009), Information theoretic measures for clusterings comparison: is a correction for chance necessary?, in ‘Proceedings of the 26th Annual International Conference on Machine Learning’, pp. 1073–1080.
- Wang, J., Lu, X., He, F. and Ma, F. (2020), ‘Which popular predictor is more useful to forecast international stock markets during the coronavirus pandemic: VIX vs EPU?’, *International Review of Financial Analysis* **72**, 101596.
- Wang, Z., Liang, Y. and Ji, P. (2020), ‘Spectral algorithms for community detection in directed networks’, *Journal of Machine Learning Research* **21**(153), 1–45.
- White, A. P. and Liu, W. Z. (1994), ‘Bias in information-based measures in decision tree induction’, *Machine Learning* **15**, 321–329.
- Wilms, I., Rombouts, J. and Croux, C. (2021), ‘Multivariate volatility forecasts for stock market indices’, *International Journal of Forecasting* **37**(2), 484–499.
- Witten, D. M., Tibshirani, R. and Hastie, T. (2009), ‘A penalized matrix decomposition, with applications to sparse principal components and canonical correlation analysis’, *Biostatistics* **10**(3), 515–534.
- Xu, K. S. and Hero, A. O. (2014), ‘Dynamic stochastic blockmodels for time-evolving social networks’, *IEEE Journal of Selected Topics in Signal Processing* **8**(4), 552–562.
- Ye, C., Wilson, R. C., Comin, C. H., Costa, L. d. F. and Hancock, E. R. (2014), ‘Approximate von Neumann entropy for directed graphs’, *Physical Review E* **89**(5), 052804.
- Yin, H., Safikhani, A. and Michailidis, G. (2023), ‘A general modeling framework for network autoregressive processes’, *Technometrics* pp. 1–11.
- Zhang, Y., Ma, F. and Liao, Y. (2020), ‘Forecasting global equity market volatilities’, *International Journal of Forecasting* **36**(4), 1454–1475.
- Zhu, X. and Pan, R. (2020), ‘Grouped network vector autoregression’, *Statistica Sinica* **30**(3), 1437–1462.

- Zhu, X., Pan, R., Li, G., Liu, Y. and Wang, H. (2017), ‘Network vector autoregression’, *The Annals of Statistics* **45**(3), 1096–1123.
- Zhu, X., Wang, W., Wang, H. and Härdle, W. K. (2019), ‘Network quantile autoregression’, *Journal of Econometrics* **212**(1), 345–358.
- Zhu, X., Xu, G. and Fan, J. (2023), ‘Simultaneous estimation and group identification for network vector autoregressive model with heterogeneous nodes’, *Journal of Econometrics* p. 105564.

A Proofs

A.1 Proof of the main theory

Proof of Lemma 4.1. The SVAR (22) can be written as an augmented VAR(1) whose transition matrix is

$$\underbrace{F}_{qs p^* \times qs p^*} = \begin{pmatrix} \Psi_1 & \Psi_2 & \dots & \Psi_{p^*-1} & \Psi_{p^*} \\ I_{qs} & 0 & \dots & 0 & 0 \\ 0 & I_{qs} & \dots & 0 & 0 \\ \vdots & \vdots & \ddots & \vdots & \vdots \\ 0 & 0 & \dots & I_{qs} & 0 \end{pmatrix}. \quad (35)$$

From the condition (i) in Assumption A.1, we can obtain the recursive relationship between its eigenvalue $\lambda(F)$ of F in (35) and corresponding eigenvectors $u = (u'_1, \dots, u'_{p^*})'$, $u_h \in \mathbb{R}^{qs}$, by

$$\begin{aligned} \lambda(F)u_{p^*} &= u_{p^*-1}, \\ \lambda(F)u_{p^*-1} &= u_{p^*-2}, \\ &\vdots \\ \lambda(F)u_2 &= u_1 \\ \lambda(F)u_1 &= \sum_{h=1}^{p^*} \Psi_h^* u_h, \end{aligned}$$

which leads to

$$\lambda(F)^{p^*} u_{p^*} = \sum_{h=1}^{p^*} \Psi_h^* u_h = \left(\sum_{h=1}^{p^*} \lambda(F)^{p^*-h} \Psi_h^* \right) u_{p^*}. \quad (36)$$

We focus on the spectral radius of F . Here, to avoid a confusion from $\|\cdot\|$ with ℓ_2 norm of a vector, we use the notation $\rho(F) = \max_i |\lambda_i(F)|$. Since the largest eigenvalue of F is equivalent to the p^* th root of the largest eigenvalue of $\sum_{h=1}^{p^*} \lambda(F)^{p^*-h} \Psi_h^*$, one has

$$\rho(F)^{p^*} = \rho \left(\sum_{h=1}^{p^*} (\pm \rho(F))^{p^*-h} \Psi_h^* \right) \leq \left\| \sum_{h=1}^{p^*} (\pm \rho(F))^{p^*-h} \Psi_h^* \right\| \leq \sum_{h=1}^{p^*} \rho(F)^{p^*-h} \|\Psi_h^*\|. \quad (37)$$

Note that by Lemma A.1, $\|(\Phi_0^*)^{-1}\| = 1$ so that

$$\|\Psi_h^*\| \leq \|(\Phi_0^*)^{-1} \Phi_h^*\| \leq \|(\Phi_0^*)^{-1}\| \|\Phi_h^*\| \leq \|\Phi_h^*\|.$$

This also implies $\rho(F) = \rho(G)$ since

$$\begin{aligned} F &= \begin{pmatrix} (\Phi_0^*)^{-1} \Phi_1^* & (\Phi_0^*)^{-1} \Phi_2^* & \dots & (\Phi_0^*)^{-1} \Phi_{p^*-1}^* & (\Phi_0^*)^{-1} \Phi_{p^*}^* \\ (\Phi_0^*)^{-1} \Phi_0^* & 0 & \dots & 0 & 0 \\ 0 & (\Phi_0^*)^{-1} \Phi_0^* & \dots & 0 & 0 \\ \vdots & \vdots & \ddots & \vdots & \vdots \\ 0 & 0 & \dots & (\Phi_0^*)^{-1} \Phi_0^* & 0 \end{pmatrix} \\ &= \underbrace{((\Phi_0^*)^{-1} \otimes I_{p^*}) \begin{pmatrix} \Phi_1^* & \Phi_2^* & \dots & \Phi_{p^*-1}^* & \Phi_{p^*}^* \\ \Phi_0^* & 0 & \dots & 0 & 0 \\ 0 & \Phi_0^* & \dots & 0 & 0 \\ \vdots & \vdots & \ddots & \vdots & \vdots \\ 0 & 0 & \dots & \Phi_0^* & 0 \end{pmatrix}}_{:=G}. \end{aligned}$$

By combining Lemma A.2 and the condition (ii) in Assumption A.1, $\rho(F)^{p^*}$ in (37) is bounded by

$$\begin{aligned} \rho(F)^{p^*} &\leq \sum_{h=1}^{p^*} \rho(G)^{p^*-h} \|\Phi_h^*\| \leq \sum_{h=1}^{p^*} \rho(G)^{p^*-h} \sum_{m=1}^s \phi_{h,s,m} = \sum_{h=1}^{p^*} \rho(G)^{p^*-h} \phi(h) \\ &\leq \phi(p^*) + \rho(G)\phi(p^*-1) + \dots + \rho(G)^{p^*-1} \phi(1) < 1. \end{aligned}$$

Hence, the system (19), equivalent to the ScBM-PVAR (3) with (9), is stable. \blacksquare

Proof of Lemma 4.2. Fix m . Define

$$Z_m = \begin{pmatrix} Y'_m \\ Y'_{s+m} \\ \vdots \\ Y'_{(N-1)s+m} \end{pmatrix}, \quad E_m = \begin{pmatrix} \varepsilon'_m \\ \varepsilon'_{s+m} \\ \vdots \\ \varepsilon'_{(N-1)s+m} \end{pmatrix}, \quad X_m = \begin{pmatrix} X'_{0,m} \\ X'_{1,m} \\ \vdots \\ X'_{(N-1),m} \end{pmatrix} \quad (38)$$

be $N \times q$, $N \times q$, $N \times qp_m$ random matrices respectively, where

$$X_{n,m} = (Y'_{ns+m-1}, \dots, Y'_{ns+m-p_m})', \quad n = 0, 1, \dots, N-1, \quad (39)$$

are $qp_m \times 1$ random vectors. The regression equation for all seasons then forms matrix seemingly unrelated equations (e.g., Chapter 4 in Hayashi; 2011),

$$Z := \begin{pmatrix} Z_1 \\ Z_2 \\ \vdots \\ Z_s \end{pmatrix} := XB + E = \begin{pmatrix} X_1 & 0 & \dots & 0 \\ 0 & X_2 & \dots & 0 \\ \vdots & \vdots & \ddots & \vdots \\ 0 & 0 & \dots & X_s \end{pmatrix} \begin{pmatrix} B_1 \\ B_2 \\ \vdots \\ B_s \end{pmatrix} + \begin{pmatrix} E_1 \\ E_2 \\ \vdots \\ E_s \end{pmatrix}. \quad (40)$$

Then the ordinary least square (OLS) estimator of the ScBM-PVAR model (3) is $q \sum_m p_m \times q$ -dimensional matrix,

$$\hat{B} = \left(\frac{1}{N} X'X \right)^{-1} \left(\frac{1}{N} X'Z \right) := \Sigma_X^{-1} \Sigma_{ZX}. \quad (41)$$

By applying Lemma A.2 in Guðmundsson and Brownlees (2021), we have

$$\lambda_1(\hat{\Sigma}_X) \geq \lambda_1(\Sigma_X) - \mathcal{O}\left(\sqrt{\frac{q}{N}}\right)$$

with probability at least $1 - 3e^{-q} \sum_m p_m$. Hence, the OLS estimator of the ScBM-PVAR (41) exists. Now let

$$\Sigma = \begin{pmatrix} \Sigma_Z & \Sigma_{ZX} \\ \Sigma'_{ZX} & \Sigma_X \end{pmatrix},$$

and $\hat{\Sigma}$ be the sample analog of Σ . By Lemma A.2 in Guðmundsson and Brownlees (2021) again,

$$\|\hat{\Sigma} - \Sigma\| = \mathcal{O}\left(\sqrt{\frac{q}{N}} \|\Sigma\|\right) \quad (42)$$

holds with probability at least $1 - 3e^{-q} \sum_m (p_m^{p_m+1})$. This leads to

$$\|\hat{\Sigma}_{ZX} - \Sigma_{ZX}\| \leq \|\hat{\Sigma} - \Sigma\| = \mathcal{O}\left(\sqrt{\frac{q}{N}} \|\Sigma\|\right), \quad (43)$$

$$\|\hat{\Sigma}_X^{-1} - \Sigma_X^{-1}\| \leq \|\hat{\Sigma}_X^{-1}\| \|\hat{\Sigma}_X - \Sigma_X\| \|\Sigma_X^{-1}\| = \mathcal{O}\left(\sqrt{\frac{q}{N}} \|\Sigma\| \|\Sigma_X^{-1}\|\right). \quad (44)$$

Combined with (43) and (44), $\|\hat{B} - B\|$ in (42) has an upper bound

$$\|\hat{B} - B\| = \mathcal{O}\left(\sqrt{\frac{q}{N}} \|\Sigma_{ZX}\| \|\Sigma\| \|\Sigma_X^{-1}\|\right) \leq \mathcal{O}\left(\sqrt{\frac{q}{N}} \|\Sigma_Z\| \|\Sigma_X\| \|\Sigma_{ZX}\| \|\Sigma_X^{-1}\|\right) = \mathcal{O}\left(\sqrt{\frac{q}{N}} \|\Sigma_X\| \|\Sigma_X^{-1}\| \|B\|\right). \quad (45)$$

By using Lemma OA. 13 in Guðmundsson and Brownlees (2021), one can show that $\|\Sigma_X\|$ and $\|\Sigma_X^{-1}\|$ are bounded. So, (45) becomes

$$\|\hat{B} - B\| = \mathcal{O}\left(\sqrt{\frac{q}{N}} \left\| \sum_{m=1}^s \sum_{h=1}^{p_m} \Phi_{h,m} \right\| \right), \quad (46)$$

since $\|B\| \leq \left\| \sum_{m=1}^s \sum_{h=1}^{p_m} \Phi_{h,m} \right\|$. Since $\|\hat{\Phi} - \Phi\| = \|\hat{B} - B\|$ and $\left\| \sum_{h=1}^{p_m} \Phi_{h,m} \right\| \leq \sum_{m=1}^s \phi_{hs,m}$, the stability condition of the ScBM-PVAR (3) leads to $\sum_{h=1}^{p_m^*} \sum_{m=1}^s \phi_{hs,m} < 1$, the upper bound of (46) yields

$$\|\hat{\Phi} - \Phi\| \leq \mathcal{O}\left(\sqrt{\frac{q}{N}}\right)$$

with the union bound probability $1 - 3e^{-q} \sum_m (p_m + 1)$. ■

Proof of Corollary 4.2. By connecting (4) – (6), we have

$$\begin{aligned}
Z &:= \begin{pmatrix} Y'_{23} \\ Y'_{24} \\ \vdots \\ Y'_T \end{pmatrix} = \begin{pmatrix} Y^{(d)'}_{22} & Y^{(w)'}_{22} & Y^{(m)'}_{22} \\ Y^{(d)'}_{23} & Y^{(w)'}_{23} & Y^{(m)'}_{23} \\ \vdots & \vdots & \vdots \\ Y^{(d)'}_{T-1} & Y^{(w)'}_{T-1} & Y^{(m)'}_{T-1} \end{pmatrix} \begin{pmatrix} \Phi^{(d)} \\ \Phi^{(w)} \\ \Phi^{(m)} \end{pmatrix} + \begin{pmatrix} \varepsilon'_{23} \\ \varepsilon'_{24} \\ \vdots \\ \varepsilon'_T \end{pmatrix} \\
&= \begin{pmatrix} Y'_{22} & \frac{1}{5} \sum_{h=0}^4 Y'_{22-h} & \frac{1}{22} \sum_{h=0}^{21} Y'_{22-h} \\ Y'_{23} & \frac{1}{5} \sum_{h=0}^4 Y'_{23-h} & \frac{1}{22} \sum_{h=0}^{21} Y'_{23-h} \\ \vdots & \vdots & \vdots \\ Y'_{T-1} & \frac{1}{5} \sum_{h=0}^4 Y'_{T-1-h} & \frac{1}{22} \sum_{h=0}^{21} Y'_{T-1-h} \end{pmatrix} \begin{pmatrix} \Phi^{(d)} \\ \Phi^{(w)} \\ \Phi^{(m)} \end{pmatrix} + \begin{pmatrix} \varepsilon'_{23} \\ \varepsilon'_{24} \\ \vdots \\ \varepsilon'_T \end{pmatrix} \\
&= \begin{pmatrix} Y'_{22} & Y'_{21} & \cdots & Y'_1 \\ Y'_{23} & Y'_{22} & \cdots & Y'_2 \\ \vdots & \vdots & \ddots & \vdots \\ Y'_{T-1} & Y'_{T-2} & \cdots & Y'_{T-22} \end{pmatrix} \begin{pmatrix} I_q & \frac{1}{5} I_q & \frac{1}{22} I_q \\ 0 & \frac{1}{5} I_q & \frac{1}{22} I_q \\ \vdots & \vdots & \vdots \\ 0 & \frac{1}{5} I_q & \frac{1}{22} I_q \\ 0 & 0 & \frac{1}{22} I_q \\ \vdots & \vdots & \vdots \\ 0 & 0 & \frac{1}{22} I_q \end{pmatrix} \begin{pmatrix} \Phi^{(d)} \\ \Phi^{(w)} \\ \Phi^{(m)} \end{pmatrix} + \begin{pmatrix} \varepsilon'_{23} \\ \varepsilon'_{24} \\ \vdots \\ \varepsilon'_T \end{pmatrix} \\
&=: XRB + E =: \tilde{X}B + E. \tag{47}
\end{aligned}$$

Then the OLS estimator of the ScBM-VHAR (4) is

$$R\hat{B} = R \left(\frac{1}{N} X'X \right)^{-1} \left(\frac{1}{N} X'Z \right) := R \Sigma_X^{-1} \Sigma_{ZX}. \tag{48}$$

Note that the estimator is a restricted form of the OLS estimator of the ScBM-VAR (1) and (8) with lag order $p = 22$. By Lemma A.2 in Guðmundsson and Brownlees (2021) for \tilde{X} yields

$$\lambda_1(\hat{\Sigma}_{\tilde{X}}) \geq \lambda_1(\Sigma_{\tilde{X}}) - \mathcal{O}\left(\sqrt{\frac{q}{N}}\right)$$

with probability at least $1 - 3e^{-22q}$. Similar to Lemma 4.1, we have

$$\|R\hat{B} - RB\| \leq \mathcal{O}\left(\sqrt{\frac{q}{N}} \|\Sigma_X\| \|\Sigma_X^{-1}\| \|RB\|\right). \tag{49}$$

Note that $\|R\|$ can be factored out for both sides so that are canceled out. For right-hand side, one can show that $\|\Sigma_X\|$ and $\|\Sigma_X^{-1}\|$ are bounded. Also since $\|B\|$ is bounded from the stability condition of the ScBM-VHAR (4) with (10), it becomes $\mathcal{O}(\sqrt{q/N})$. The left-hand side of (49) is

$$\|\hat{\Phi} - \Phi\| \leq \|R(\hat{B} - B)\|.$$

Hence, by taking the same route of the proof of Lemma 4.2, we have the desired result (28). ■

Proof of Lemma 4.3. We define the adjacency matrix $A = [A_{m,\ell}(i, j)]$ augmented along the s seasons, which is a similar construction as the placement of VAR transition matrix of (25) (see also an example of Baek et al.; 2017). For instance, for season $s = 4$ with $q = 2$, the structure of augmented adjacency matrix A corresponding to the model (25) with $s = 4, q = 2$ is

$$A = \begin{pmatrix} & & & & & & A_{1,1}(1, 1) & A_{1,2}(1, 2) \\ & & & & & & A_{1,1}(2, 1) & A_{1,2}(2, 2) \\ A_{2,1}(1, 1) & A_{2,1}(1, 2) & & & & & & \\ A_{2,1}(2, 1) & A_{2,1}(2, 2) & & & & & & \\ & & A_{3,1}(1, 1) & A_{3,1}(1, 2) & & & & \\ & & A_{3,1}(2, 1) & A_{3,1}(2, 2) & & & & \\ & & & & A_{4,1}(1, 1) & A_{4,1}(1, 2) & & \\ & & & & A_{4,1}(2, 1) & A_{4,1}(2, 2) & & \end{pmatrix}. \tag{50}$$

Similar to the alignment of block components in the adjacency matrix A , the adjacency matrix of the population \mathcal{A} and corresponding autoregressive matrices A and \tilde{A} and corresponding matrices from stacked VAR transition matrices Φ and $\tilde{\Phi}$ are defined similarly. With the defined matrices, one has their symmetrized matrices by

$$\tilde{\Phi}^S := \begin{pmatrix} 0 & \tilde{\Phi} \\ \tilde{\Phi}' & 0 \end{pmatrix}, \quad \Phi^S := \begin{pmatrix} 0 & \Phi \\ \Phi' & 0 \end{pmatrix}.$$

Then one has

$$\|\Phi^S - \tilde{\Phi}^S\| \leq \|\tilde{\Phi}^S - \tilde{C}^S\| + \|\tilde{C}^S - \Phi^S\|, \quad (51)$$

where $\tilde{C} = (\mathcal{O}^\tau)^{-1/2} A' (\mathcal{P}^\tau)^{-1/2}$ and \mathcal{O} and \mathcal{P} are formed by \mathcal{O}_m^τ and \mathcal{P}_m^τ with the same placement as A . Assume that \tilde{C}^S is defined similarly as \tilde{L}^S, L^S . In addition, let $\tilde{A} = [\tilde{A}_{m,\ell}(i,j)]$ where $\tilde{A}_{m,\ell}(i,j) \in \{0,1\}$ and $A_{m,\ell}(i,j) = [w_m]_{ij} \tilde{A}_{m,\ell}(i,j)$ with $[w_m]_{ij}$ defined in Section 2. Similarly, we can also define its population analog $\tilde{\mathcal{A}}_{m,\ell}(i,j) = [\omega_m]_{ij} \tilde{\mathcal{A}}_{m,\ell}(i,j)$.

Consider the first term (51). Define

$$W_{m,s+\ell}(i, q+j) = \frac{([w_m]_{ij} \tilde{A}_{m,\ell}(i,j) - [\omega_m]_{ij} \tilde{\mathcal{A}}_{m,\ell}(i,j)) E_{m,s+\ell}(i, q+j)}{\sqrt{([\mathcal{O}_m]_{ii} + \tau_m)([\mathcal{P}_m]_{jj} + \tau_m)}}$$

be the random variable as a sum of random variables $E_{m,s+\ell}(i, q+j)$ where the entries that the subscript and superscript indicates in $w\tilde{A}$ and its corresponding symmetrized counterpart in $(w\tilde{A})'$, respectively, and so do $\omega\tilde{\mathcal{A}}$ and $(\omega\tilde{\mathcal{A}})'$. Note that $\mathbb{E}[W_{m,s+\ell}(i, q+j)] = 0$ and

$$\begin{aligned} & \mathbb{E}W_{m,s+\ell}(i, q+j)^2 \\ &= \frac{E_{m,m}(i, i) + E_{s+\ell, s+\ell}(q+j, q+j)}{([\mathcal{O}_m]_{ii} + \tau_m)([\mathcal{P}_m]_{jj} + \tau_m)} \left((\mu_m^2 + \sigma_m^2) \tilde{\mathcal{A}}_{m,\ell}(i, j)(1 - \tilde{\mathcal{A}}_{m,\ell}(i, j)) + \sigma_m^2 \tilde{\mathcal{A}}_{m,\ell}(i, j) \right) \\ &\leq \frac{E_{m,m}(i, i) + E_{s+\ell, s+\ell}(q+j, q+j)}{([\mathcal{O}_m]_{ii} + \tau_m)([\mathcal{P}_m]_{jj} + \tau_m)} \tilde{\mathcal{A}}_{m,\ell}(i, j)(\mu_m^2 + \sigma_m^2). \end{aligned}$$

Define $\delta_m + \tau_m$ by

$$\frac{1}{\sqrt{([\mathcal{O}_m]_{ii} + \tau_m)([\mathcal{P}_m]_{jj} + \tau_m)}} \leq \frac{1}{\delta_m + \tau_m},$$

where $\delta_m = \min(\min_i [\mathcal{O}_m]_{ii}, \min_j [\mathcal{P}_m]_{jj})$. Take $\max_m \mu_m^2 + \sigma_m^2 = c_1$ and $\min \delta_m + \tau_m = \delta + \tau = c_2$. Then

$$\begin{aligned} v^2 &= \left\| \sum_{m=1}^s \sum_{\ell=1}^s \sum_{i=1}^q \sum_{j=1}^q \mathbb{E}W_{m,s+\ell}(i, q+j)^2 \right\| \\ &= \max \left[\max_{m=1, \dots, s} \left\{ \max_{i=1, \dots, q} \left(\sum_{j=1}^q \frac{E_{m,m}(i, i) + E_{s+\ell, s+\ell}(q+j, q+j)}{([\mathcal{O}_m]_{ii} + \tau_m)([\mathcal{P}_m]_{jj} + \tau_m)} \tilde{\mathcal{A}}_{m,\ell}(i, j)(\mu_m^2 + \sigma_m^2) \right), \right. \right. \\ &\quad \left. \max_{j=1, \dots, q} \left(\sum_{i=1}^q \frac{E_{m,m}(i, i) + E_{s+\ell, s+\ell}(q+j, q+j)}{([\mathcal{O}_m]_{ii} + \tau_m)([\mathcal{P}_m]_{jj} + \tau_m)} \tilde{\mathcal{A}}_{m,\ell}(i, j)(\mu_m^2 + \sigma_m^2) \right) \right\}, \\ &\quad \max_{\ell=1, \dots, s} \left\{ \max_{i=1, \dots, q} \left(\sum_{j=1}^q \frac{E_{m,m}(i, i) + E_{s+\ell, s+\ell}(q+j, q+j)}{([\mathcal{O}_m]_{ii} + \tau_m)([\mathcal{P}_m]_{jj} + \tau_m)} \tilde{\mathcal{A}}_{m,\ell}(i, j)(\mu_\ell^2 + \sigma_\ell^2) \right), \right. \\ &\quad \left. \max_{j=1, \dots, q} \left(\sum_{i=1}^q \frac{E_{m,m}(i, i) + E_{s+\ell, s+\ell}(q+j, q+j)}{([\mathcal{O}_m]_{ii} + \tau_m)([\mathcal{P}_m]_{jj} + \tau_m)} \tilde{\mathcal{A}}_{m,\ell}(i, j)(\mu_\ell^2 + \sigma_\ell^2) \right) \right\} \right] \\ &\leq \max \left[\max_{m=1, \dots, s} \frac{\mu_m^2 + \sigma_m^2}{\delta_m + \tau_m} \left\{ \max_{i=1, \dots, q} \left(\sum_{j=1}^q \frac{\tilde{\mathcal{A}}_{m,\ell}(i, j)}{[\mathcal{O}_m]_{ii} + \tau_m} \right), \max_{j=1, \dots, q} \left(\sum_{i=1}^q \frac{\tilde{\mathcal{A}}_{m,\ell}(i, j)}{[\mathcal{P}_m]_{jj} + \tau_m} \right) \right\}, \right. \\ &\quad \left. \max_{\ell=1, \dots, s} \frac{\mu_\ell^2 + \sigma_\ell^2}{\delta_\ell + \tau_\ell} \left\{ \max_{i=1, \dots, q} \left(\sum_{j=1}^q \frac{\tilde{\mathcal{A}}_{m,\ell}(i, j)}{[\mathcal{O}_m]_{ii} + \tau_m} \right), \max_{j=1, \dots, q} \left(\sum_{i=1}^q \frac{\tilde{\mathcal{A}}_{m,\ell}(i, j)}{[\mathcal{P}_m]_{jj} + \tau_m} \right) \right\} \right] \\ &= \max_m \frac{\mu_m^2 + \sigma_m^2}{\delta_m + \tau_m} \leq \frac{\max_m (\mu_m^2 + \sigma_m^2)}{\min_m (\delta_m + \tau_m)} = \frac{c_1}{c_2}. \end{aligned}$$

By using Lemma E.1 in Rohe et al. (2016) (same as Matrix Bernstein inequality; Theorem 5.4.1 in Vershynin (2018)),

$$\mathbb{P}(\|\tilde{C}^S - \tilde{\Phi}^S\| \geq a) \leq 4sq \exp\left(\frac{-a^2}{2v^2 + 2(c_1/c_2)a/3}\right),$$

Take

$$a = \sqrt{\frac{3c_1 \log(8sq/\epsilon)}{c_2}} < 1$$

by controlling $\epsilon > 0$. Then we have

$$\mathbb{P} \left(\|\tilde{C}^S - \tilde{\Phi}^S\| \leq a \right) \geq 1 - 4sq \exp \left(-\frac{3 \log(8sq/\epsilon)}{3} \right) \geq 1 - \frac{\epsilon}{2}. \quad (52)$$

Next, consider the second term in (51). Define

$$\tilde{D}^S = \begin{pmatrix} O^\tau & 0 \\ 0 & P^\tau \end{pmatrix}, \quad D^S = \begin{pmatrix} O^\tau & 0 \\ 0 & P^\tau \end{pmatrix}.$$

and $\tilde{D}_\tau^S, D_\tau^S$ be the regularized analogs of \tilde{D}^S, D^S . Note that from (7), the entry at season m in the larger matrix \tilde{D}_τ^S is

$$[\tilde{D}_{m,\tau}^S]_{ii} = \sum_{j=1}^q [\mathcal{A}_m]_{ij} = \mu_m [\Theta_m^y]_{ii} \sum_{j=1}^q [B_m]_{y_i z_j} [\Theta_m^z]_{jj}, \text{ or } \sum_{i=1}^q [\mathcal{A}_m]_{ij} = \mu_m [\Theta_m^z]_{jj} \sum_{i=1}^q [B_m]_{y_i z_j} [\Theta_m^y]_{ii},$$

and each diagonal entries defined independently of the other entries. Therefore, by the definition of minimum degree for all seasons $\tau + \delta$, Assumption 29 is also satisfied in \tilde{D}_τ^S and D_τ^S . Note also that $\|\Phi^S\| \leq \sqrt{\frac{c_1}{c_2}}$. This gives us

$$\begin{aligned} \|\tilde{C}^S - \Phi^S\| &= \|(\tilde{D}_\tau^S)^{-1/2} (D_\tau^S)^{1/2} \Phi^S (D_\tau^S)^{1/2} (\tilde{D}_\tau^S)^{-1/2} - \Phi^S\| \\ &= \|((\tilde{D}_\tau^S)^{-1/2} (D_\tau^S)^{1/2} - I_{2sq}) \Phi^S (D_\tau^S)^{1/2} (\tilde{D}_\tau^S)^{-1/2} + \Phi^S ((\tilde{D}_\tau^S)^{-1/2} (D_\tau^S)^{1/2} - I_{2sq})\| \\ &\leq \|(\tilde{D}_\tau^S)^{-1/2} (D_\tau^S)^{1/2} - I_{2sq}\| \|\Phi^S (D_\tau^S)^{1/2} (\tilde{D}_\tau^S)^{-1/2}\| + \|L_m^S ((\tilde{D}_\tau^S)^{-1/2} (D_\tau^S)^{1/2} - I_{2sq})\| \\ &\leq \|(\tilde{D}_\tau^S)^{-1/2} (D_\tau^S)^{1/2} - I_{2sq}\| \|\Phi^S\| \| (D_\tau^S)^{1/2} (\tilde{D}_\tau^S)^{-1/2} \| + \|\Phi^S\| \|(\tilde{D}_\tau^S)^{-1/2} (D_\tau^S)^{1/2} - I_{2sq}\| \\ &\leq \sqrt{\frac{c_1}{c_2}} \|(\tilde{D}_\tau^S)^{-1/2} (D_\tau^S)^{1/2} - I_{2sq}\| \|((D_m^S)^{1/2} (\tilde{D}_\tau^S)^{-1/2} - I_{2sq}) + I_{2sq}\| + \sqrt{\frac{c_1}{c_2}} \|(\tilde{D}_\tau^S)^{-1/2} (D_\tau^S)^{1/2} - I_{2sq}\| \\ &\leq \sqrt{\frac{c_1}{c_2}} \|(\tilde{D}_\tau^S)^{-1/2} (D_\tau^S)^{1/2} - I_{2sq}\|^2 + 2\sqrt{\frac{c_1}{c_2}} \|(\tilde{D}_\tau^S)^{-1/2} (D_\tau^S)^{1/2} - I_{2sq}\| \\ &\leq 3\sqrt{\frac{c_1}{c_2}} \|(\tilde{D}_\tau^S)^{-1/2} (D_\tau^S)^{1/2} - I_{2sq}\|. \end{aligned}$$

Since $D_\tau^S, \tilde{D}_\tau^S$ have only one non-zero entry at each row and column,

$$\begin{aligned} \|(\tilde{D}_\tau^S)^{-1/2} (D_\tau^S)^{1/2} - I_{2sq}\| &\leq \sqrt{\|(\tilde{D}_\tau^S)^{-1/2} (D_\tau^S)^{1/2} - I_{2sq}\|_1 \|(\tilde{D}_\tau^S)^{-1/2} (D_\tau^S)^{1/2} - I_{2sq}\|_\infty} \\ &= \sqrt{\max_{j=1,\dots,2sq} \sum_{i=1}^{2sq} \left| \sqrt{\frac{[D_\tau^S]_{ij}}{[\tilde{D}_\tau^S]_{ij}}} - 1 \right| \sqrt{\max_{i=1,\dots,2sq} \sum_{j=1}^{2sq} \left| \sqrt{\frac{[D_\tau^S]_{ij}}{[\tilde{D}_\tau^S]_{ij}}} - 1 \right|}} \\ &\leq \sqrt{\max_{j=1,\dots,2sq} \sum_{i=1}^{2sq} \left| \frac{[D_\tau^S]_{ij}}{[\tilde{D}_\tau^S]_{ij}} - 1 \right| \sqrt{\max_{i=1,\dots,2sq} \sum_{j=1}^{2sq} \left| \frac{[D_\tau^S]_{ij}}{[\tilde{D}_\tau^S]_{ij}} - 1 \right|}} \\ &\leq \sqrt{\max_{j=1,\dots,2sq} \left| \frac{[D_\tau^S]_{ij}}{[\tilde{D}_\tau^S]_{ij}} - 1 \right| \sqrt{\max_{i=1,\dots,2sq} \left| \frac{[D_\tau^S]_{ij}}{[\tilde{D}_\tau^S]_{ij}} - 1 \right|}} \\ &= \max_{j=1,\dots,2sq} \left| \frac{[D_\tau^S]_{ij}}{[\tilde{D}_\tau^S]_{ij}} - 1 \right| \leq \max_{\substack{j=1,\dots,2sq \\ m=1,\dots,s}} \left| \frac{[D^S]_{ij} + \tau_m}{[\tilde{D}^S]_{ij} + \tau_m} - 1 \right|. \end{aligned}$$

This implies that

$$\begin{aligned} \mathbb{P} \left(\|(\tilde{D}_\tau^S)^{-1/2} (D_\tau^S)^{1/2} - I_{2sq}\| \geq a\sqrt{\frac{c_2}{c_1}} \right) &\leq \mathbb{P} \left(\max_{\substack{j=1,\dots,2sq \\ m=1,\dots,s}} \left| \frac{[D^S]_{ij} + \tau_m}{[\tilde{D}^S]_{ij} + \tau_m} - 1 \right| \geq a\sqrt{\frac{c_2}{c_1}} \right) \\ &\leq \mathbb{P} \left(\bigcup_{m=1,\dots,s} \left\{ \bigcup_{j=1,\dots,2sq} \left\{ |[\tilde{D}^S]_{ii} - [D^S]_{ii}| \geq a\sqrt{\frac{c_2}{c_1}} ([D^S]_{ij} + \tau_m) \right\} \right\} \right). \end{aligned}$$

From the combination of sub-Gaussian and sub-exponential tail bounds,

$$\begin{aligned}
& \mathbb{P} \left(|[\tilde{D}^S]_{ii} - [D^S]_{ii}| \geq a\sqrt{\frac{c_2}{c_1}}([D^S]_{ij} + \tau_m) \right) \\
& \leq \exp \left(\frac{-a^2 c_2 ([D^S]_{ij} + \tau_m)^2}{2c_1 [\tilde{D}^S]_{ii}} \right) + \exp \left(\frac{-a^2 c_2 ([D^S]_{ij} + \tau_m)^2}{2c_1 [\tilde{D}^S]_{ii} + \frac{2}{3} a c_1^{1/2} c_2^{1/2} ([D^S]_{ij} + \tau_m)} \right) \\
& \leq 2 \exp \left(\frac{-a^2 c_2 ([D^S]_{ij} + \tau_m)^2}{(2c_1 + \frac{2}{3} a c_1) ([\tilde{D}^S]_{ii} + \tau)^2} \right) \leq 2 \exp \left(\frac{-a^2 c_2}{3c_1} \right) \\
& \leq 2 \exp(-\log(8sq/\epsilon)) \leq \frac{\epsilon}{4sq}.
\end{aligned}$$

Therefore,

$$\mathbb{P} \left(3\sqrt{\frac{c_1}{c_2}} \|(\tilde{D}_\tau^S)^{-1/2} (D_\tau^S)^{1/2} - I_q\| \leq 3a \right) \geq 1 - \frac{\epsilon}{2}. \quad (53)$$

Therefore, combining (52) and (53), we have for any $\epsilon > 0$,

$$\mathbb{P} \left(\|\tilde{L}^S - L^S\| \leq 4a \right) \geq 1 - \epsilon$$

if $c_1 > 3c_2 \log(8sq/\epsilon)$. Therefore, with a high probability,

$$\|\tilde{\Phi}^S - \Phi^S\| \leq \mathcal{O} \left(\sqrt{\frac{\log(sq)}{sqB_{sq}}} \right).$$

■

Proof of Lemma 4.4. Similar to (50), for example, from the adjacency matrix A with $s = 4$, we define \hat{X}_L, \hat{X}_R by

$$\hat{X}_L := \begin{pmatrix} 0 & 0 & 0 & \hat{X}_{1,L} \\ \hat{X}_{2,L} & 0 & 0 & 0 \\ 0 & \hat{X}_{3,L} & 0 & 0 \\ 0 & 0 & \hat{X}_{4,L} & 0 \end{pmatrix}, \quad \hat{X}_R := \begin{pmatrix} 0 & 0 & 0 & \hat{X}_{1,R} \\ \hat{X}_{2,R} & 0 & 0 & 0 \\ 0 & \hat{X}_{3,R} & 0 & 0 \\ 0 & 0 & \hat{X}_{4,R} & 0 \end{pmatrix}$$

and block matrices of orthogonal rotation maps \mathcal{R}_L and \mathcal{R}_R are defined similarly. From Sections 4.2.1 and 4.2.2, by taking $q/N = qs/T$, we have

$$\|\tilde{\Phi}^S - \hat{\Phi}^S\| \leq \|\tilde{\Phi}^S - \Phi^S\| + \|\Phi^S - \hat{\Phi}^S\| \leq \mathcal{O} \left(\sqrt{\frac{sq}{T}} + \sqrt{\frac{\log(sq)}{sqB_{sq}}} \right).$$

Then consider \hat{X}_L, \hat{X}_R and their population version $\mathcal{X}_L, \mathcal{X}_R$, and

$$\hat{X} = \begin{pmatrix} \hat{X}_L \\ \hat{X}_R \end{pmatrix}, \quad \mathcal{X} = \begin{pmatrix} \mathcal{X}_L \\ \mathcal{X}_R \end{pmatrix}.$$

By the Davis-Kahan theorem and Lemma OA.11 in Guðmundsson and Brownlees (2021)

$$\|\hat{X}_{m,L} \hat{X}'_{m,L} - \mathcal{X}_{m,L} \mathcal{X}'_{m,L}\| \leq \|\hat{X}_L \hat{X}'_L - \mathcal{X}_L \mathcal{X}'_L\| \leq \|\hat{X} \hat{X}' - \mathcal{X} \mathcal{X}'\| \leq \frac{\|\tilde{\Phi}^S - \hat{\Phi}^S\|}{\mu} \leq \mathcal{O} \left(\sqrt{\frac{sq}{T}} + \sqrt{\frac{\log(sq)}{sqB_{sq}}} \right),$$

for $\mu \in (0, \sum_{m=1}^s \sum_{h=1}^{p_m} \phi_{h,m}]$. Similarly,

$$\|\hat{X}_{m,R} \hat{X}'_{m,R} - \mathcal{X}_{m,R} \mathcal{X}'_{m,R}\| \leq \mathcal{O} \left(\sqrt{\frac{sq}{T}} + \sqrt{\frac{\log(sq)}{sqB_{sq}}} \right).$$

From orthogonal Procrustes problem (e.g., Schönemann; 1966),

$$\begin{aligned}
\|\hat{X}_{m,L} - \mathcal{X}_{m,L} \mathcal{R}_{m,L}\| & \leq \|\hat{X}_{m,L} \hat{X}'_{m,L} - \mathcal{X}_{m,L} \mathcal{X}'_{m,L}\|, \\
\|\hat{X}_{m,R} - \mathcal{X}_{m,R} \mathcal{R}_{m,R}\| & \leq \|\hat{X}_{m,R} \hat{X}'_{m,R} - \mathcal{X}_{m,R} \mathcal{X}'_{m,R}\|,
\end{aligned}$$

are satisfied for orthogonal rotation matrices $\mathcal{R}_{m,L}, \mathcal{R}_{m,R}$. From Lemma OA.7 in Guðmundsson and Brownlees (2021), we have

$$\begin{aligned} & \|\hat{X}_{m,L}^* - \mathcal{X}_{m,L}^* \mathcal{R}_{m,L}\| \\ &= \|\hat{Q}_{m,L} \hat{X}_{m,L} - \mathcal{Q}_{m,L} \mathcal{X}_{m,L} \mathcal{R}_{m,L}\| \\ &\leq \|\hat{Q}_{m,L} - \mathcal{Q}_{m,L}\| \|\hat{X}_{m,L} - \mathcal{X}_{m,L} \mathcal{R}_{m,L}\| + \|\hat{Q}_{m,L} - \mathcal{Q}_{m,L}\| \|\mathcal{X}_{m,L} \mathcal{R}_{m,L}\| + \|\mathcal{Q}_{m,L}\| \|\hat{X}_{m,L} - \mathcal{X}_{m,L} \mathcal{R}_{m,L}\|, \end{aligned}$$

and similarly

$$\begin{aligned} & \|\hat{X}_{m,R}^* - \mathcal{X}_{m,R}^* \mathcal{R}_{m,R}\| \\ &\leq \|\hat{Q}_{m,R} - \mathcal{Q}_{m,R}\| \|\hat{X}_{m,R} - \mathcal{X}_{m,R} \mathcal{R}_{m,R}\| + \|\hat{Q}_{m,R} - \mathcal{Q}_{m,R}\| \|\mathcal{X}_{m,R} \mathcal{R}_{m,R}\| + \|\mathcal{Q}_{m,R}\| \|\hat{X}_{m,R} - \mathcal{X}_{m,R} \mathcal{R}_{m,R}\|, \end{aligned}$$

where $[\hat{Q}_{m,L}]_{ii} = 1/\|\hat{X}_{m,L}\|_i$, $[\hat{X}_{m,R}]_{jj} = 1/\|\hat{X}_{m,R}\|_j$ and $\mathcal{Q}_{m,L}, \mathcal{Q}_{m,R}$ are their population analogs, respectively. Note that

$$\|\mathcal{X}_{m,L}\|_i = \left(\frac{[\Theta_m^{y,\tau}]_{jj}}{\sum_i [\Theta_m^{y,\tau}]_{ii}} \right)^{1/2}, \quad \|\mathcal{X}_{m,R}\|_i = \left(\frac{[\Theta_m^{z,\tau}]_{jj}}{\sum_j [\Theta_m^{z,\tau}]_{jj}} \right)^{1/2}.$$

Stack up $\{\hat{Q}_{m,L}\}_m$ and $\{\hat{Q}_{m,R}\}_m$, $m = 1, \dots, s$, as the same order as $\hat{X}_{m,L}$ and $\hat{X}_{m,R}$. Denote them by \hat{Q}_L and \hat{Q}_R . Since $\hat{Q}_{m,L}, \hat{Q}_{m,R}$ are diagonal matrices so \hat{Q}_L, \hat{Q}_R have only one non-zero entry for all pairs of rows and columns. This implies

$$\|\mathcal{Q}_L\| \leq \mathcal{O}(\sqrt{sq}), \quad \|\mathcal{Q}_R\| \leq \mathcal{O}(\sqrt{sq}).$$

Also note that

$$\|[\hat{X}_{m,L}]_{ij} - [\mathcal{X}_{m,L}]_i \cdot [\mathcal{R}_{m,L}]_{\cdot j}\| \leq \|[\hat{X}_{m,L}]_{\cdot j} - \mathcal{X}_{m,L} [\mathcal{R}_{m,L}]_{\cdot j}\| \leq \|\hat{X}_{m,L} - \mathcal{X}_{m,L} \mathcal{R}_{m,L}\|,$$

for all $i = 1, \dots, q$ and $j = 1, \dots, K_{m,y}$. Therefore,

$$\|[\hat{X}_{m,L}]_i - [\mathcal{X}_{m,L}]_i \cdot \mathcal{R}_{m,L}\| = \mathcal{O}(\|\hat{X}_{m,L} - \mathcal{X}_{m,L} \mathcal{R}_{m,L}\|).$$

By the definition of $\hat{Q}_{m,L}$ and $\mathcal{Q}_{m,L}$,

$$[\hat{Q}_{m,L}^{-1} - \mathcal{Q}_{m,L}^{-1}]_{ii} = \|[\hat{X}_{m,L}]_i\| - \|[\mathcal{X}_{m,L}]_i \cdot [\mathcal{R}_{m,L}]_{\cdot j}\| \leq \|[\hat{X}_{m,L}]_i - [\mathcal{X}_{m,L}]_i \cdot \mathcal{R}_{m,L}\| = \mathcal{O}(\|\hat{X}_{m,L} - \mathcal{X}_{m,L} \mathcal{R}_{m,L}\|).$$

For the right singular vectors, we have a similar result,

$$[\hat{Q}_{m,R}^{-1} - \mathcal{Q}_{m,R}^{-1}]_{ii} \leq \mathcal{O}(\|\hat{X}_{m,R} - \mathcal{X}_{m,R} \mathcal{R}_{m,R}\|).$$

By Lemma OA.8 in Guðmundsson and Brownlees (2021),

$$\begin{aligned} \|\hat{Q}_{m,L} - \mathcal{Q}_{m,L}\| &\leq \|\hat{Q}_{m,L}\| \|\mathcal{Q}_{m,L}^{-1} - \hat{Q}_{m,L}^{-1}\| \|\mathcal{Q}_{m,L}\| \\ &= \mathcal{O}(\|\mathcal{Q}_{m,L}\| \|\hat{X}_{m,L} - \mathcal{X}_{m,L} \mathcal{R}_{m,L}\|) = \mathcal{O}(\sqrt{q} \|\hat{X}_{m,L} - \mathcal{X}_{m,L} \mathcal{R}_{m,L}\|), \end{aligned}$$

as $\|\hat{Q}_{m,L}\|$ is close to $\hat{Q}_{m,L}$ for large q . For s -block matrix \hat{Q}_L , by the same reasoning,

$$\|\hat{Q}_L - \mathcal{Q}_L\| \leq \mathcal{O}(\sqrt{sq} \|\hat{X}_{m,L} - \mathcal{X}_{m,L} \mathcal{R}_{m,L}\|).$$

For the right singular vectors, we have a similar result,

$$\|\hat{Q}_R - \mathcal{Q}_R\| \leq \mathcal{O}(\sqrt{sq} \|\hat{X}_{m,R} - \mathcal{X}_{m,R} \mathcal{R}_{m,R}\|).$$

Therefore, we have

$$\|\hat{X}_L^* - \mathcal{X}_L^* \mathcal{R}_L\| + \|\hat{X}_R^* - \mathcal{X}_R^* \mathcal{R}_R\| = \mathcal{O}\left(\frac{sq}{\sqrt{T}} + \sqrt{\frac{\log(sq)}{Bsq}}\right),$$

where $\mathcal{R}_L, \mathcal{R}_R$ are stacks of $\{\mathcal{R}_{m,L}\}_m$ and $\{\mathcal{R}_{m,R}\}_m$, $m = 1, \dots, s$, by the same order as \hat{X}_L, \hat{X}_R . This result holds with the same probability as Lemmas 4.2 and 4.3. \blacksquare

Proof of Lemma 4.4. First consider the clustering for input Y_m , $m = 1, \dots, s$. By following Rohe et al. (2016), define the sets of nodes Y -misclutered at season m by

$$\mathcal{N}_m^y = \{i : \|[\hat{C}_{m,L}]_i - [C_{m,L}]_i\|_2 > \|[\hat{C}_{m,L}]_j - [C_{m,L}]_j\|_2 \text{ for any } i \neq j\}.$$

Since all population centroids are of unit length and are orthogonal to each other, by using the proof of Theorem 4.4 in Qin and Rohe (2013),

$$\|[\hat{C}_{m,L}]_i - [C_{m,L}]_i\|_2 < 1/\sqrt{2} \Rightarrow \|[\hat{C}_{m,L}]_i - [C_{m,L}]_i\|_2 > \|[\hat{C}_{m,L}]_j - [C_{m,L}]_j\|_2, \text{ for all } j \neq i.$$

This implies that

$$\mathcal{N}_m^y \subset \mathcal{B}_m^y = \{i : \|[\hat{C}_{m,L}]_i - [C_{m,L}]_i\|_2 \geq 1/\sqrt{2}\}.$$

Recall that for each season m , finding k_m clustering points from k -means clustering is equivalent to solve

$$\min_{M_1, \dots, M_{K_m}} \sum_i \min_r \|[\hat{X}_{m,L}]_i - M_r\|_2^2. \quad (54)$$

For the centroid, the solution of (54), $M_1^*, \dots, M_{K_m}^*$, write them in a matrix form $M_{m,L}^*$ which only has k_m different rows. Then we have

$$\|\hat{X}_{m,L}^* - \hat{C}_{m,L}\|_F \leq \|\hat{X}_{m,L}^* - M_{m,L}^*\|_F \leq \|\hat{X}_{m,L}^* - \mathcal{X}_{m,L}^* \mathcal{R}_{m,L}\|_F.$$

By the triangle inequality,

$$\begin{aligned} \|\hat{C}_{m,L} - C_{m,L}\|_F &= \|\hat{C}_{m,L} - \mathcal{X}_{m,L}^* \mathcal{R}_{m,L}\|_F \\ &\leq \|\hat{X}_{m,L}^* - \hat{C}_{m,L}\|_F + \|\hat{X}_{m,L}^* - \mathcal{X}_{m,L}^* \mathcal{R}_{m,L}\|_F \\ &\leq 2\|\hat{X}_{m,L}^* - \mathcal{X}_{m,L}^* \mathcal{R}_{m,L}\|_F. \end{aligned}$$

Therefore,

$$\begin{aligned} \frac{1}{s} \sum_{m=1}^s \frac{|\mathcal{N}_m^y|}{q} &\leq \frac{1}{s} \sum_{m=1}^s \frac{|\mathcal{B}_m^y|}{q} = \frac{1}{sq} \sum_{m=1}^s \sum_{i \in \mathcal{B}_{m,L}} 1 \leq \frac{2}{sq} \sum_{m=1}^s \sum_{i \in \mathcal{B}_{m,L}} \|[\hat{C}_{m,L}]_i - [C_{m,L}]_i\|_2^2 \\ &= \frac{2}{sq} \sum_{m=1}^s \|\hat{C}_{m,L} - C_{m,L}\|_F^2 \leq \frac{8}{sq} \sum_{m=1}^s \|\hat{X}_{m,L}^* - \mathcal{X}_{m,L}^* \mathcal{R}_{m,L}\|_F^2 = \frac{8}{sq} \|\hat{X}_L^* - \mathcal{X}_L^* \mathcal{R}_L\|_F^2. \end{aligned} \quad (55)$$

Next, consider the clustering for output Z_m , $m = 1, \dots, s$. Similar to the input cases, define the set of nodes Z -misclustered at season m by

$$\mathcal{N}_m^z = \{i : \|[\hat{C}_{m,R}]_i - [C_{m,R}]_i\|_2 > \|[\hat{C}_{m,R}]_j - [C_{m,R}]_j\|_2 \text{ for any } i \neq j\}.$$

In addition to a similar reasoning, without loss of generality, assume $K_m = K_{y_m} \leq K_{z_m}$. Also,

$$[\mathcal{O}_m]_{ii} = \sum_{k=1}^q [\mathcal{A}'_m]_{ik} = \mu_m [\Theta_m^y]_{ii} \sum_{k=1}^q [\Theta_m^z]_{kk} [B_m]_{y_k y_k} = \mu_m [\Theta_m^y]_{ii} [B_m]_{y_i y_i},$$

similarly,

$$[\mathcal{P}_m]_{ii} = \sum_{k=1}^q [\mathcal{A}'_m]_{kj} = \mu_m [\Theta_m^z]_{jj} [B_m]_{z_j z_j}.$$

From $\mathcal{O}_m^\tau = \mathcal{O}_m + \tau_m I_q$ and $\mathcal{P}_m^\tau = \mathcal{P}_m + \tau_m I_q$,

$$[\Theta_m^{y,\tau}] = \Theta_m^y \frac{[\mathcal{O}_m]_{ii}}{[\mathcal{O}_m]_{ii} + \tau_m}, \quad [\Theta_m^{z,\tau}] = \Theta_m^z \frac{[\mathcal{P}_m]_{jj}}{[\mathcal{P}_m]_{jj} + \tau_m}.$$

This gives the expression of the population graph Laplacian

$$\begin{aligned} (\mathcal{O}_m^\tau)^{-1/2} \mathcal{A}'_m (\mathcal{P}_m^\tau)^{-1/2} &= (\Theta_m^{y,\tau})^{1/2} Y_m \left(\sum_k [B_m]_{rk} \right)^{-1/2} B_m \left(\sum_k [B_m]_{ks} \right)^{-1/2} Z'_m (\Theta_m^{z,\tau})^{1/2} \\ &=: (\Theta_m^{y,\tau})^{-1/2} Y_m B_{L,m} Z'_m (\Theta_m^{z,\tau})^{1/2}. \end{aligned}$$

In addition to a similar reasoning, we assumed $K_m = K_{m,y} \leq K_{m,z}$. Here, we adjust the term to reflect the impact of the shrunk community number. Define

$$H_m = (Y'_m \Theta_m^{y,\tau} Y_m)^{1/2} B_{L,m} (Z'_m \Theta_m^{z,\tau} Z_m)^{1/2} \in \mathbb{R}^{K_{m,y} \times K_{m,z}}.$$

Note that H_m shares the same top k_m singular values with the population graph Laplacian at season m . This can be written as

$$H_m = U_m \Lambda_m V'_m$$

Lemma A.2 For Φ_h^* defined as (21), $\|\Phi_h^*\| \leq \phi(h) = \sum_{m=1}^s \phi_{hs,m}$, where $\phi(h)$ are defined in the condition (ii) in Assumption A.1.

Proof: Let $\sigma(A)$ be a set of eigenvalues of the matrix A . For a fixed h , define

$$\mathcal{G}_{h,m} := \sigma(\Phi_{hs,m}) \cup \left\{ \lambda \notin \sigma(\Phi_{hs,m}) \mid \|(\Phi_{hs,m} - \lambda I_q)^{-1}\|^{-1} \leq \sum_{\substack{m'=1 \\ m' \neq m}}^s \|\Phi_{hs,m'}\| \right\}.$$

Then by Theorem 2.7 in Salas (1999), $\sigma(\Phi_h^*) \in \cup_{m=1}^s \mathcal{G}_{h,m}$. By using triangular inequality, this implies

$$\rho(\Phi_h^*) \leq \max_m \left(\|\Phi_{hs,m}\| + \sum_{\substack{m'=1 \\ m' \neq m}}^s \|\Phi_{hs,m'}\| \right) \leq \sum_{m=1}^s \phi_{hs,m} = \phi(h), \quad (57)$$

where $\phi_{hs,m}$ and $\phi(h)$ are defined in the condition (ii) in Assumption A.1, and the last inequality of (57) holds due to Lemma OA.12 in Guðmundsson and Brownlees (2021). ■

B Additional tables and figures for Data applications

B.1 Application of ScBM-PVAR

Category	Level 2 Subcategory	Level 3 Subcategory	Code
Total Private	Goods-Producing Mining and Logging Construction Manufacturing	- Durable Goods	Mining
		- Nondurable Goods	Construction Durable Nondurable
Private	Service-Provision Trade, Transportation, and Utilities	- Wholesale Trade	Wholesale
		- Retail Trade	Retail
	- Transportation and Warehousing	Transportation	
	- Utilities	Utility	
	Information Financial Activities	- Finance and Insurance	Information
		- Real Estate and Rental and Leasing	Finance RealEstate
	Professional and Business Services	- Professional, Scientific, and Technical Services	Professional
		- Management of Companies and Enterprises	Management
	Private Education and Health Services	- Administrative and Support and Waste Management and Remediation Services	Administration
		- Private Educational Services	Education
Leisure and Hospitality	- Health Care and Social Assistance	HealthCare	
	- Arts, Entertainment, and Recreation	Arts	
Other Services	- Accommodation and Food Services	Accommodation	
		Other	
Government	Federal State Government Local Government		Federal State Local

Table C1: Hierarchy of Industry Sectors in Nonfarm Payroll Employment.

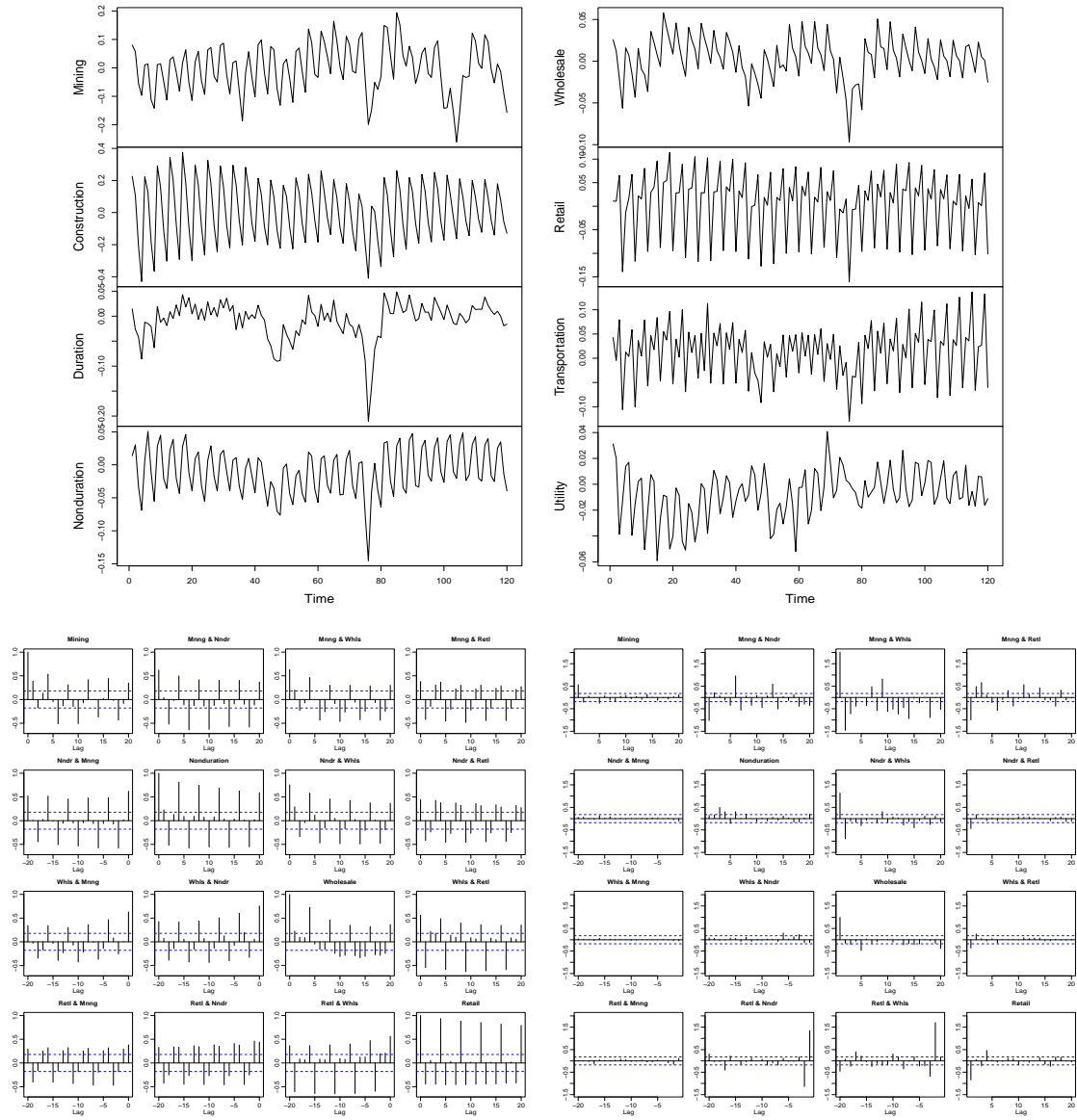


Figure C1: (Top) Time plots of the first eight time series (see Table C1 for code). (Left Bottom) Sample ACF plots for selected sectors (Mining, Nondurable, Wholesale, and Retail). (Right Bottom) Sample PACF plots for the same sectors.

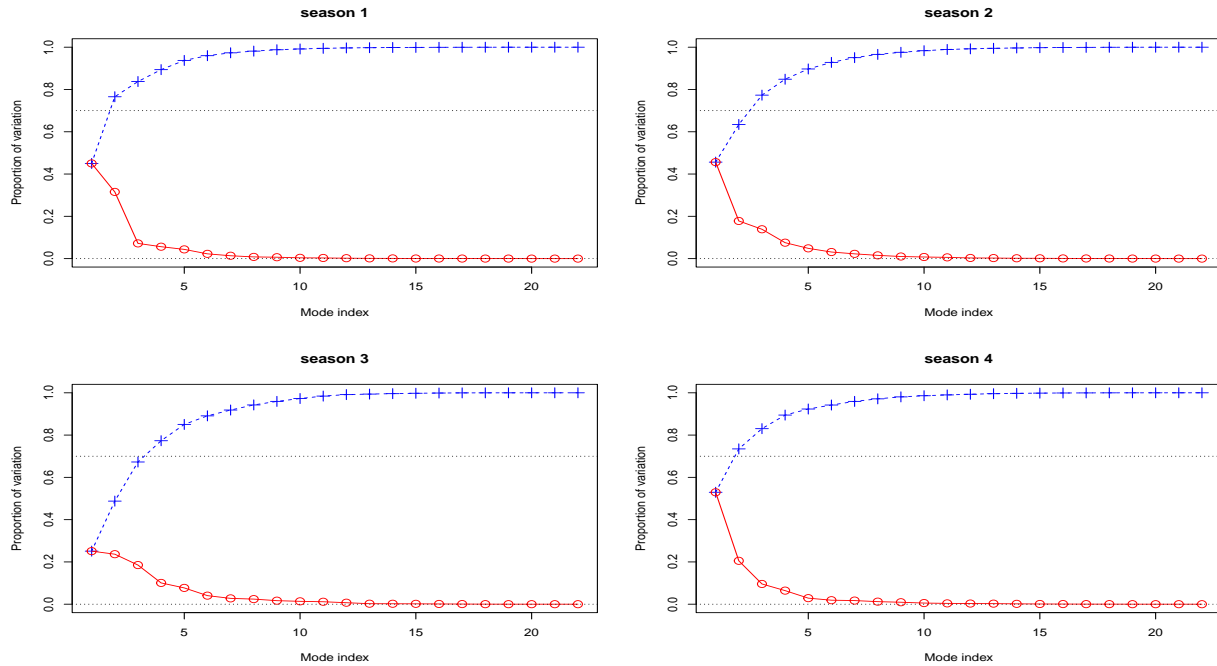


Figure C2: Scree plots of singular values from the estimated transition matrices of ScBM-PVAR with four seasons. The red solid curves represent the proportion of variation explained by each singular value, while the blue dashed curves indicate the cumulative proportion. The black dotted lines mark the 70% threshold.

B.2 Application of ScBM-VHAR

Stock Index	Market	Continent	MSCI Classification	Ticker
S&P 500	United States	North America	Developed	GSPC
FTSE 100	United Kingdom	Europe	Developed	FTSE
Nikkei 225	Japan	Asia	Developed	N225
DAX	Germany	Europe	Developed	GDAXI
Russell 2000	United States	North America	Developed	RUT
All Ordinaries	Australia	Oceania	Developed	AORD
DJIA	United States	North America	Developed	DJI
Nasdaq 100	United States	North America	Developed	NDX
CAC 40	France	Europe	Developed	FCHI
Hang Seng	Hong Kong	Asia	Developed	HSI
KOSPI Composite Index	South Korea	Asia	Developed	KS11
AEX Index	Netherlands	Europe	Developed	AEX
Swiss Market Index	Switzerland	Europe	Developed	SSMI
IBEX 35	Spain	Europe	Developed	IBEX
S&P CNX Nifty (Nifty 50)	India	Asia	Emerging	NSEI
IPC Mexico	Mexico	North America	Emerging	MXX
Bovespa Index	Brazil	South America	Emerging	BVSP
S&P/TSX Composite Index	Canada	North America	Developed	GSPTSE
Euro STOXX 50	Eurozone	Europe	Developed	STOXX50E
FTSE MIB	Italy	Europe	Developed	FTSEMIB.MI

Table C2: The list of 20 stock indices with their regions of markets, continents, MSCI market classification, and ticker symbols.

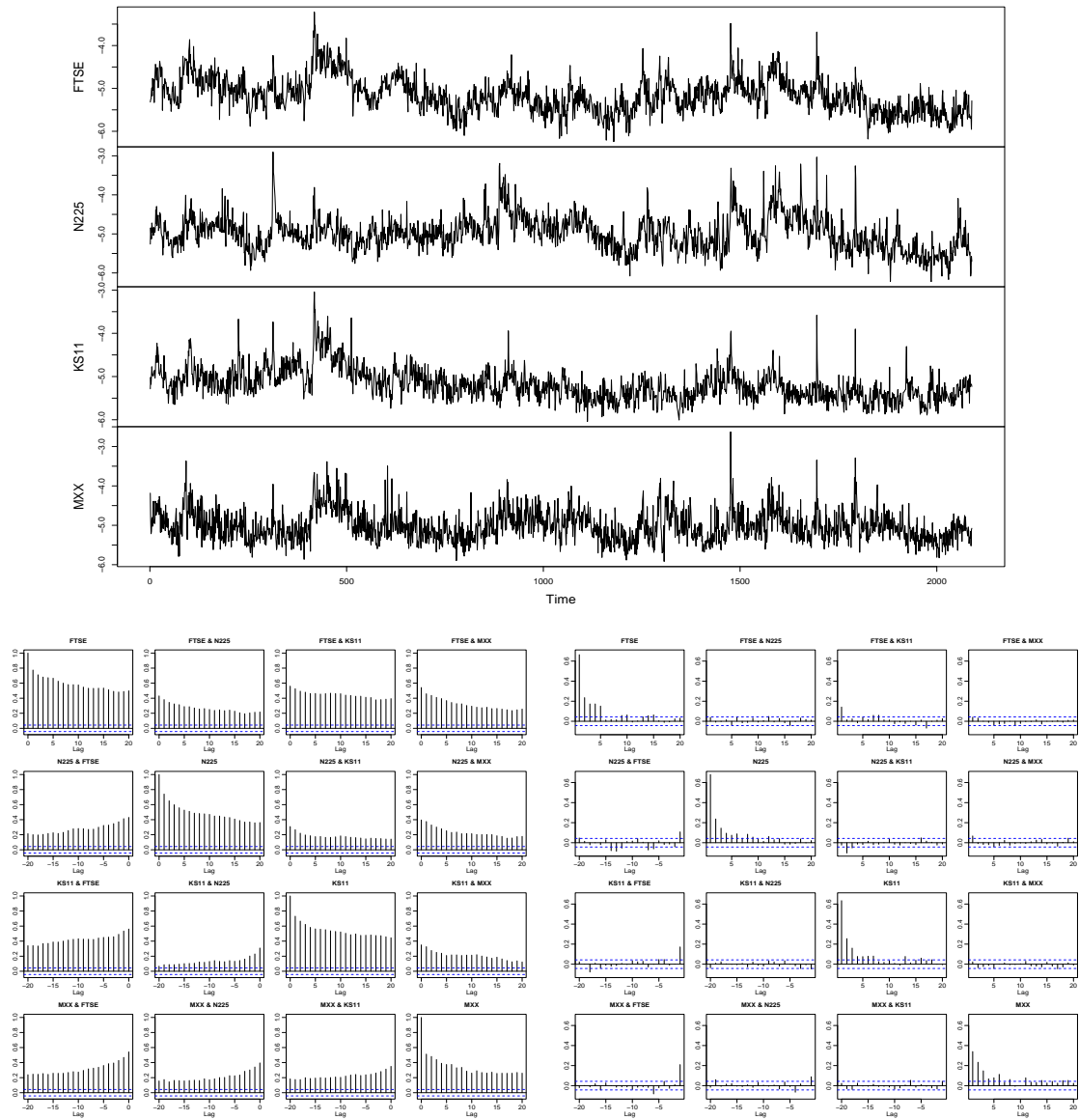


Figure C3: (Top) Time plots of four selected stock indices (FTSE 100, Nikkei 225, KOSPI Composite Index, and IPC Mexico). (Bottom Left) Sample ACF plots of the series. (Bottom Right) Sample PACF plots of the series.

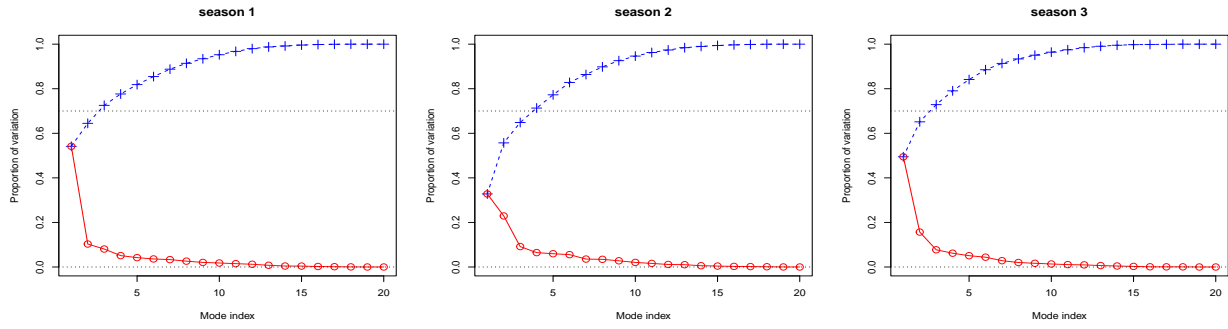


Figure C4: Scree plots of singular values from the estimated transition matrices of ScBM-VHAR with daily, weekly, and monthly effects. The red solid curves represent the proportion of variation explained by each singular value, while the blue dashed curves indicate the cumulative proportion. The black dotted lines mark the 70% threshold.